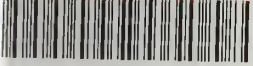


Reference

NBS
Publi-
cations

NAT'L INST. OF STAND & TECH

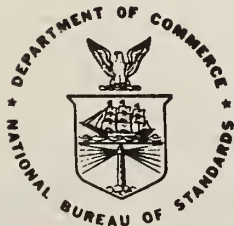


11106 259738 IR 82-2471

CS1: A Two-Dimensional Finite Element Charge-Sheet Model of A Short-Channel MOS Transistor

U.S. DEPARTMENT OF COMMERCE
National Bureau of Standards
National Engineering Laboratory
Center for Electronics and
Electrical Engineering
Semiconductor Devices & Circuits Division
Washington, DC 20234

April 1982



QC

100

.U56

82-2471

1982

DEPARTMENT OF COMMERCE

NATIONAL BUREAU OF STANDARDS

NATIONAL BUREAU
OF STANDARDS
LIBRARY

MAY 14 1982

Not a - Key
34100
1250
NBS-2471
1982

NBSIR 82-2471

**CS1: A TWO-DIMENSIONAL FINITE
ELEMENT CHARGE-SHEET MODEL OF A
SHORT-CHANNEL MOS TRANSISTOR**

C. L. Wilson and J. L. Blue

U.S. DEPARTMENT OF COMMERCE
National Bureau of Standards
National Engineering Laboratory
Center for Electronics and
Electrical Engineering
Semiconductor Devices & Circuits Division
Washington, DC 20234

April 1982

U.S. DEPARTMENT OF COMMERCE, Malcolm Baldrige, *Secretary*
NATIONAL BUREAU OF STANDARDS, Ernest Ambler, *Director*

Table of Contents

	Page
Abstract	1
1. Introduction	2
2. Theory	3
A. Two-Dimensional Charge-Sheet Model	3
B. Numerical Procedures	6
3. Computer Implementation	9
A. Software Modules	9
B. Physical Restrictions	11
4. Device Model Verification	13
5. Conclusions	31
Acknowledgments	31
References	32
Appendix A. Channel Current Calculation	34
Appendix B. File CS1.HLP	35
Appendix C. File CS1.EXP	40

List of Figures

	Page
1. The geometry used in the charge-sheet model	5
2. a) Two-dimensional level 2 mesh for the 1.12- μm transistor	14
b) Two-dimensional equipotentials for the 1.12- μm transistor	15
3. Convergence of the direct method for the test problem	18
4. Convergence of the multigrid method for the test problem	19
5. Relationship between the surface potential change and the Newton step size for the test problem	20
6. a) Relationship between surface potential change (kT/q) and drain current change (arbitrary unit, $J_D = 1$) for the level 1 mesh	21
b) Relationship between surface potential change (kT/q) and drain current change (arbitrary unit, $J_D = 1$) for the level 2 mesh	22

List of Figures (continued)	Page
7. Comparison of the drain current calculated by the one- and two-dimensional models	24
8. Comparison of the subthreshold and triode region drain current measured and calculated using the one- and two-dimensional models .	25
9. Comparison of the triode region drain current measured and calculated using the one- and two-dimensional models	27
10. Comparison of the output characteristics measured and calculated using the two-dimensional model for the 3.20- μm transistor	28
11. a) Comparison of the output characteristics measured and calculated using the two-dimensional model for a 1.89- μm transistor .	29
b) Comparison of the output characteristics measured and calculated using the one-dimensional model for a 1.89- μm transistor .	30
C-1. Example of level 1 mesh	50
C-2. Example of level 2 mesh	51
C-3. Example of level 3 mesh	52
C-4. Example of level 1 projection	53
C-5. Example of level 2 projection	54
C-6. Example of level 3 projection	55
C-7. Example of contour plot	56

List of Tables

	Page
1. Available Computer Types	12
2. Transistor Parameters	12
3. Iteration Convergence	16

CS1: A Two-Dimensional Finite Element Charge-Sheet Model
of a Short-Channel MOS Transistor

C. L. Wilson and J. L. Blue*
National Bureau of Standards
Washington, DC 20234

Abstract

A two-dimensional charge-sheet model for short-channel MOS transistors has been developed. The unique feature of the model is that the effect of channel inversion layer charge is included as a non-linear integral boundary condition on the two-dimensional electrostatic field in the transistor. The average inversion layer charge density and source-drain current are obtained directly from the model rather than from the electron density or electron quasi-Fermi level. The model retains all of the physical detail of more complex two-dimensional models such as sensitivity to source-drain profile shape, channel profile, and oxide field shape. This allows the model to represent the changes in drain current associated with short-channel effects while still allowing simple comparison with long-channel models. For long-channel transistors, the results of this model are identical to Brews' long-channel charge-sheet model. The accuracy of this model is verified by modeling a sequence of transistors with channel lengths between 4.6 and 1.1 μm . In short-channel transistors, effects previously attributed to high field mobility are explained by simple two-dimensional electrostatics.

The simulations produced using this model have been compared to experimental measurements on an array of n-channel MOSFETs; the model is in good agreement for transistors with channel lengths as short as 1.1 μm . In this verification process, the model represented accurately the onset of subthreshold current, channel-length-induced threshold voltage offset, and drain-field-induced output conductance changes.

From studies of numerical accuracy, we conclude that the charge-sheet model can easily simulate drain current with an accuracy which exceeds that required for most applications. To obtain 5-percent accuracy for drain current, a 146 element mesh is sufficient. Refinement of the 146 element mesh to a 455 element mesh gives a current which is accurate to 0.16 percent. Average computer time for a high accuracy solution is 2.5 min on a DEC-20.[†]

The numerical solutions were obtained using general-purpose software for solving elliptic partial differential equations. Problems

* NBS Center for Applied Mathematics, Scientific Computing Division.

† Certain commercial equipment, instruments, or materials are identified in this paper in order to adequately specify the experimental procedure. Such identification does not imply recommendation or endorsement by the National Bureau of Standards, nor does it imply that the materials or equipment identified are necessarily the best available for the purpose.

with exact solutions have been solved to test the correctness and accuracy of the codes. Also, the physics included in this model and the geometry of the transistor can be easily changed. The finite element method used allows refinement of oblique triangles which is important in achieving computational efficiency. The program is portable and has been run on a DEC-20, a VAX 11/780, a Cyber 175, and a Univac 1108.*

Key words: elliptic solvers; finite elements; interactive graphics; MOS transistor.

1. Introduction

A two-dimensional formulation of a charge-sheet model of an MOS transistor and an associated computer program is presented. This formulation differs from the formulation of De La Moneda [1] in that it includes the effects of source-drain channel shape and arbitrary channel doping profile shape. The formulation differs from the formulation proposed by Brews [2] in that strong two-dimensional electrostatic effects are included by solving Poisson's equation using adaptive finite element techniques in the bulk semiconductor. In this formulation, a new approach that differs from both [1] and [2] is used to couple the one-dimensional current flow to the two-dimensional potential. The effects of the charge in the inverted channel of the transistor is included as a nonlinear boundary condition at the interface between the semiconductor and the gate oxide. This formulation allows the two-dimensional electrostatic field and drain current to be calculated without the inclusion of an additional two-dimensional current continuity equation. This results in a great improvement in computational efficiency which allows finite element model calculations to be performed on a minicomputer. This model is accurate in all regions of inverted transistor operation and works well even in regions of operation where the channel current produces large changes in the electrostatic potential in the channel. The model retains the computational efficiency of single equation models [3] without imposing the computer requirements of coupled equation models [4,5,6]. The complexity and cost of the model lies between the long-channel one-dimensional model of Brews, which runs well on a desk top calculator, and the coupled equation models, which are best suited to large computers. Unlike previous single equation models [3], the two-dimensional charge-sheet model works in all regions of inverted transistor operation including weak inversion. Use of the finite-element method also allows the adaptive mesh procedures [7] previously applied to MESFETs [8] to be applied to MOSFETs.

In section two, the formulation of the two-dimensional charge-sheet model and the integral boundary condition at the semiconductor-oxide interface are discussed. In this formulation, the total channel current is computed as a function of the two-dimensional electrostatic potential. The computation of total channel current allows the effects of this mobile charge to be treated as an effective surface charge and to be included in subsequent calculations of the electrostatic potential as a nonlinear integral boundary condition.

In section two, the numerical procedures used to calculate the electrostatic potential in two dimensions with a nonlinear boundary condition are also discussed. The partial differential equation is transformed into a system of

nonlinear equations using adaptive, computer-generated, finite elements. The nonlinear field equations are solved using a damped Newton's method. The resultant system of linear equations is solved either by direct methods or by a multigrid iteration.

In section three, the specific procedures used to implement the model are discussed. The structure of the computer program is discussed and the function of each of the principal modules is outlined. The installation requirements of the program are discussed as are the sources of the software components which were developed by other authors. The physical limitations of the model are then discussed. These simplifications are responsible for the low cost of the model but may, in some cases, lead to modeling inaccuracies. Solutions to these physical limitations are outlined.

In section four, the modeling of an array of MOS transistors is discussed. First, the numerical accuracy of the model is discussed. Next, the relationship between long-channel theory, as represented by the one-dimensional charge-sheet model, and the two-dimensional model is discussed. Using the two-dimensional model, it is possible to obtain accurate models of transistors with channel lengths less than 1.0 μm . The transistors used in this work have a nominal channel doping density of $1 \times 10^{15} \text{ cm}^{-3}$. This low channel doping density increases short-channel effects by increasing the Debye length in the channel of the transistor. If, for example, transistors with channel doping density of $1 \times 10^{16} \text{ cm}^{-3}$ had been used, then short-channel effects comparable to those seen in the 1.12- μm transistor would occur in a transistor with 0.35- μm channel length. In reference [9], the onset of short-channel effects is calculated for the subthreshold region; a transistor is classified as short channel if excess subthreshold current is present. For the channel doping and oxide thickness used in this study, this short-channel limit is at 5.6 μm ; all of the transistors studied are short-channel transistors from a subthreshold current criterion.

2. Theory

A. Two-Dimensional Charge-Sheet Model

The general form of the static semiconductor device equations is given by reference [10]:

$$\nabla^2 \psi = -\rho/\epsilon \quad (1)$$

$$\rho = q(N_d + p - n)$$

$$n = n_i e^{q(\psi - \phi_n)/kT} \quad (2)$$

$$p = n_i e^{q(\phi_p - \psi)/kT} \quad (3)$$

$$\nabla \cdot (\mu_n n \nabla \phi_n) = R \quad (4)$$

$$\nabla \cdot (\mu_p p \nabla \phi_p) = -R, \quad (5)$$

where ψ is the electrostatic potential; ρ is the net space charge density; ϵ is the dielectric permittivity; N_d is the net ionized impurity density; n and p are the electron and hole densities; n_i is the intrinsic carrier density; ϕ_n, ϕ_p are the quasi-Fermi levels; μ_n, μ_p are the electron and hole mobilities; and R is the net volume generation-recombination rate. The coordinate system used in these calculations is shown in figure 1. The source-and-drain regions of the device are assumed to be uniform at the source or drain potential and are removed from the calculation. This improves the stability of the calculation by removing two regions in which space charge neutrality is achieved by subtracting a large mobile carrier density from a large doping density. This geometry was discussed previously in reference [10]. If recombination is neglected and the model is explicitly restricted to n-channel transistors by neglecting hole current, then eqs (1) to (5) become:

$$\nabla^2 \psi = q(n - N_d)/\epsilon \quad (6)$$

$$\nabla \cdot \left[\mu_n n_i \exp(q(\psi - \phi_n)/kT) \nabla \phi_n \right] = 0 \quad (7)$$

so that the electron current density is given by:

$$J_n = q \mu_n n_i \exp\left(\frac{q(\psi - \phi_n)}{kT}\right) \nabla \phi_n. \quad (8)$$

If eq (6) is used in both the oxide and semiconductor regions of the transistor, then an interior constraint must be imposed at the oxide-semiconductor interface:

$$\epsilon_{ox} \frac{\partial \psi}{\partial x} \Big|_{o-} - \epsilon_{sc} \frac{\partial \psi}{\partial x} \Big|_{o+} = -Q \quad (9)$$

where ϵ_{ox} and ϵ_{sc} are the permittivities of the gate oxide and the semiconductor, respectively; the subscripts $o+, o-$ represent the two sides of the interface; and Q is the total net interface surface charge density. The inclusion of these dielectric effects would require modification of eq (1):

$$\nabla \cdot (\epsilon \nabla \psi) = -\rho. \quad (10)$$

An alternate approach, used here, is to separate the transistor into oxide and semiconductor regions and use eq (9) as a matching boundary condition.

Direct solution of eqs (6) and (7) is possible, and several methods exist for doing this [4,5,6]. In surface channel transistors, with or without implanted channels, the electron current is concentrated in a thin sheet near the semiconductor-oxide interface. If eq (6) is solved in two dimensions to obtain $\psi(x,y)$, then this interface-associated charge is given by:

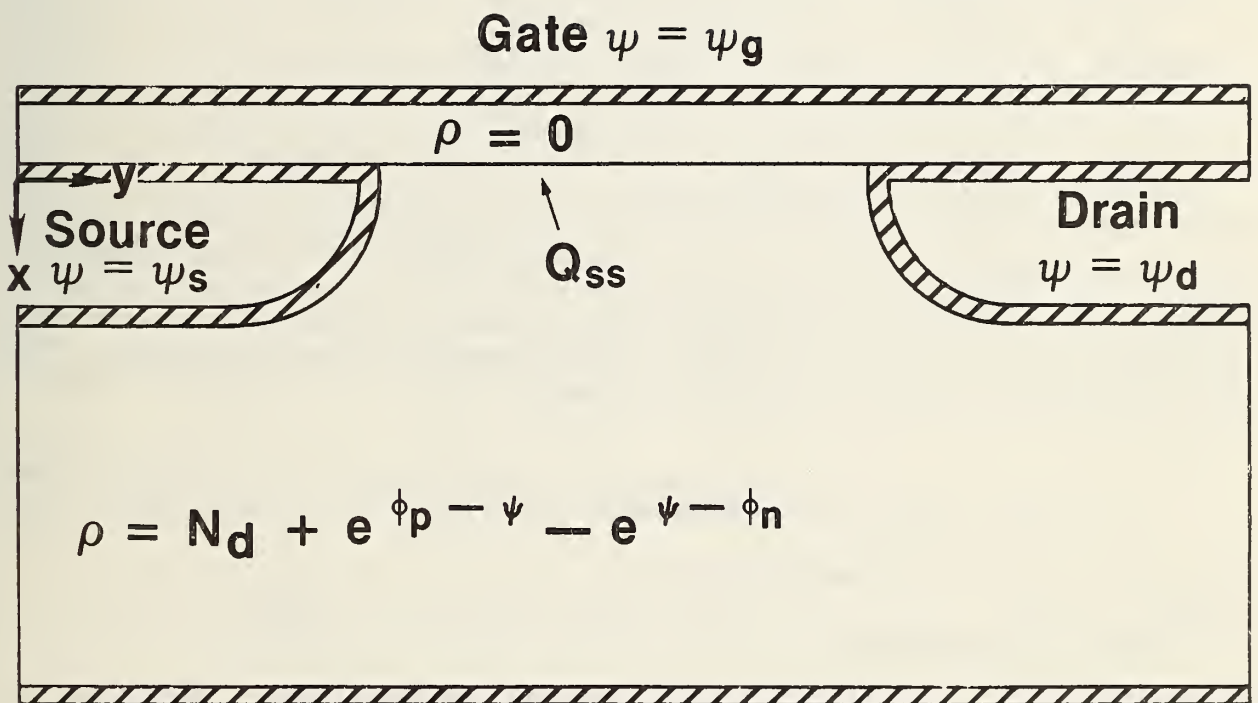


Figure 1. The geometry used in the charge-sheet model.

$$N(y) = \frac{n_i}{\mu_n^*} \int_0^\infty dx e^{\beta\psi} \mu_n \left\{ 1 + [e^{-\beta V_d} - 1] \frac{\int_0^y \frac{dy_0}{\int_0^\infty dx e^{\beta\psi} \mu_n}}{\int_0^L \frac{dy_0}{\int_0^\infty dx e^{\beta\psi} \mu_n}} \right\} \quad (11)$$

and the total electron current in the channel is given by:

$$I = \frac{Wq n_i}{\beta} \frac{[e^{-\beta V_d} - 1]}{\int_0^L \frac{dy_0}{\int_0^\infty dx e^{\beta\psi} \mu_n}} \quad (12)$$

where $\beta = q/kT$, the weighted mobility is given by $\mu_n^* = \frac{1}{L} \int_0^L \mu_n dy$, V_d is the source-drain voltage, L is the channel length, and W is the channel width. The derivation of these equations is given in Appendix A. The charge calculated in eq (12) is used in eq (9) to combine the competing effects of gate surface inversion and inversion charge screening caused by current. The two-dimensional charge-sheet model is given by eqs (6), (9), and (11) where Q in eq (9) is:

$$Q = Q_{\text{surface}} + q N(y) \quad (13)$$

and drain current is given by eq (12).

B. Numerical Procedures

An important feature of this work is that the numerical solutions were obtained using general-purpose software for solving elliptic partial differential equations (PDEs). Although some efficiency is sacrificed, the benefits obtained by using the general-purpose software far outweigh the loss in efficiency. Problems with exact solutions have been solved to test the correctness and accuracy of the codes and to determine optimal strategies and optimal values for parameters in the code. The physics included in the model and the geometry of the problem can be easily changed. The numerical software was inspired by finite-element software of Bank and Sherman [7] and retains most of their philosophy. Currently, a general-purpose package to solve coupled nonlinear systems of time-dependent partial differential equations is being developed. The current report uses an intermediate version of the package.

This version of the package solves the PDE

$$\nabla \cdot [a(x, y, u) \nabla u] = f \left(x, y, u, \frac{\partial u}{\partial x}, \frac{\partial u}{\partial y} \right) \quad (14)$$

in a region bounded by straight line segments and circular arc segments. On each segment of the boundary, u must obey one of two types of boundary conditions:

$$(1) \quad g(x, y, u) = 0 \quad (15)$$

$$(2) \quad \partial u / \partial n + g(x, y, u) = 0 \quad (16)$$

This is a fairly general example of a PDE arising from conservation of a flux and includes both Poisson's equation and the hole and electron continuity equations (in the multiple-PDE version).

At the heart of the package is a module which solves a linear elliptic PDE using linear finite elements on a mesh of triangles. (Boundary "triangles" may have one curved side.) The initial triangulation is an input to the package; succeeding triangulations are calculated adaptively by the package.

For a given triangulation with M vertices, the calculation proceeds as follows. The M finite-element basis functions $\{b_m\}$ are linear on each triangle; b_m is 1 at vertex m and 0 at all other vertices. The set of vertices on type 1 boundaries is denoted by D (for Dirichlet). The solution is approximated by a sum of basis functions

$$u(x, y) = \sum_{m=1}^M \alpha_m b_m(x, y) \quad (17)$$

The coefficients are determined by a Galerkin method [11]; the error in the PDE is made orthogonal to each of the basis functions except those in D .

$$\iint \left[(-\nabla \cdot (a \nabla u) + f) b_m = 0, \right]_{\substack{m=1, 2, \dots, M \\ m \text{ not in } D}} \quad (18)$$

The remaining conditions on the b 's are that the type 1 boundary conditions hold exactly [11].

$$g(x_m, y_m, u(x_m, y_m)) = 0, \quad m \text{ in } D \quad (19)$$

Equation (18) is integrated by parts to yield

$$\iint (a \nabla u \cdot \nabla b_m + f b_m) + \int_2 a g b_m = 0 \quad (20)$$

where the single integral is over the type-2 parts of the boundary only. Equations (19) and (20) comprise M nonlinear equations in M unknowns, the coefficients $\{\alpha_m\}$.

The M nonlinear equations are solved by an iterative process, a damped Newton's method. Let v be the Newton step and use a fraction of v as a correction to u; v has the same form as u,

$$v(x,y) = \sum_{m=1}^M \beta_m b_m(x,y) . \quad (21)$$

To calculate v, we replace u by u + v in eqs (19) and (20) and linearize in v. The linearization of eq (19) yields

$$\alpha_m + \frac{\partial g(x_m, y_m, u_m)}{\partial u} \beta_m = 0, \quad m \text{ in } D , \quad (22)$$

and the linearization of eq (20) yields

$$\begin{aligned} & \iint \left\{ a \nabla v \cdot \nabla b_m + \frac{\partial a}{\partial u} v \nabla u \cdot \nabla b_m \right. \\ & \quad \left. + b_m \left(\frac{\partial f}{\partial u} v + \frac{\partial f}{\partial(\partial u / \partial x)} \frac{\partial v}{\partial x} + \frac{\partial f}{\partial(\partial u / \partial y)} \frac{\partial v}{\partial y} \right) \right\} \\ & \quad + \int_2 \left(g \frac{\partial a}{\partial u} + a \frac{\partial g}{\partial u} \right) b_m = \\ & \quad - \iint \left(a \nabla u \cdot \nabla b_m + f b_m \right) - \int_2 a g b_m \equiv r_m . \end{aligned} \quad (23)$$

Substituting for u and v from eqs (17) and (21) and doing the integrals numerically gives a set of M linear equations for the correction coefficients $\{\beta_m\}$. These linear equations are sparse; there are typically only nine nonzero elements per row, on average, and M can be a few hundred or a few thousand. A satisfactory way to solve these equations is directly, with Gaussian Elimination, using the Yale Sparse Matrix Package [12].

Unless u is close to a solution of the nonlinear finite-element equations, u + v may be worse than u. A damped Newton's method is used: replace u by u + λv, where λ is chosen so that $\max_m |r_m(u + v)| < \max_m |r_m(u)|$. This avoids divergence of the iterative process.

In practice, the initial triangulation may be too coarse to give the desired accuracy or may need local refinement to represent the solution accurately in a region of high curvature. After the package has converged to an approximate solution on the initial triangulation, the approximate solution may be used to estimate the error and produce a new and finer triangulation adaptively. There are various ways to approximate the error in each triangle. For the present work, a simple method is used. In the silicon, the PDE is

$$\nabla^2 \psi = -\rho/\epsilon . \quad (24)$$

Since ψ is linear in each triangle, $\nabla^2\psi = 0$. We estimate the relative error in each triangle by

$$\left| \int_{\text{triangle}} \rho(x,y) \right| . \quad (25)$$

The refined triangulation is obtained by dividing the triangles with the largest estimated errors, such as all triangles with estimated error larger than 1/4 of the largest error.

For the refined triangulation, the previously calculated u is a good guess at the new u , so that few Newton iterations should be necessary. The hardest work is done on the initial triangulation, the one with the fewest vertices.

If there are two or more triangulations, the linear equations on the finest triangulation may be solved by a multilevel iteration [13,7], saving both time and storage space. However, for the present problem, sufficient accuracy could be obtained with M of only a few hundred, so that a direct solution using the Yale Sparse Matrix Package was quite adequate.

Using this procedure, the solution of eqs (9) to (11) is started by first obtaining a trial solution for the linearized form of eq (10), using the solution of eq (11) obtained from the one-dimensional charge-sheet model with eq (9) as a boundary condition. The Jacobian of g required for the solution of eq (22) contains the Jacobian of eq (11). This Jacobian is approximated by

$$\frac{\partial g}{\partial u} = q\beta N(y) . \quad (26)$$

Once the surface charge and approximate local field term are obtained from the one-dimensional model and a local-field condition, the field term in eq (9) associated with the oxide is obtained using a fast Poisson solver [14]. The trial solution is then used to obtain a solution for eq (11) by quadrature and an additional fast Poisson solution in the oxide. This iterative procedure is repeated for each Newton step until the requested convergence is obtained or the specified maximum iteration count is reached.

3. Computer Implementation

A. Software Modules

The distributed source of the CS1 program is divided into four files: CS1.FOR, SYSTEM.FOR, PDESUB.FOR, and DEVLIB.FOR. These four files are ANSI 66 FORTRAN IV and can be compiled on any FORTRAN compiler which meets this standard. The files CS1.HLP, CS1.EXP, and CS1.LNK are also provided. CS1.HLP provides a set of user instructions identical to Appendix B of this report. CS1.EXP contains an example set of program input and output which is identical to Appendix C of this report. The file CS1.LNK is a sample set of linkage control statements which have been used to link the program on the DEC TOPS-20 system.

The file CS1.FOR is the actual charge-sheet model program. This file contains the subroutines which control input and output, model initial approximations, the oxide field solution, and the calls to the subroutines which solve the partial differential equation. The starting approximation is identical to the charge-sheet model originally developed by Brews in [2]. The output of this long-channel model is printed at the beginning of each CS1 calculation. The oxide solution is calculated using the fast methods discussed in reference [14]; these subroutines are in the file DEVLIB.FOR. A complete copy of the Swarztrauber and Sweet package is not included. Only those parts of the package that are used by CS1 are included.

The CS1 module of the program contains parameters TOL and IP(6) which are used to control the accuracy of the solution. The parameter TOL is used to control the iteration accuracy at each multigrid level. The parameter IP(6) is used to control the number of multigrid levels. These parameters are set to yield very accurate solutions in the version of the program which is distributed. This level of accuracy greatly exceeds that required for most applications, but is necessary, during installation and testing, to verify that the program has been correctly installed. Resetting these parameters to lower accuracy by increasing the iteration tolerance and/or decreasing the number of multigrid levels will greatly improve run times.

The file SYSTEM.FOR contains subroutines which are used in the other three program files but which are system dependent. The subroutines FOPEN and FCLOSE are used to open and close input and output files. In the DEC TOPS-20 version supplied on the tape, the file FCLOSE is a dummy subroutine. The subroutines ISTEIME and IFTIME are used to start and stop clocks which are used to measure the execution times of the parts of the partial differential solution process. If these routines are not used and dummy subroutines are substituted, ISTEIME must be less than, NOT equal to, IFTIME. If these subroutines are dummy routines, then the timing information in the output summary will be incorrect.

The subroutines PLTUTL, CURVEA, and ISCALE contain calls to vector graphics subroutines. The calls in the supplied program can be used with the TCS software supplied by Tektronix* and can be used to drive either Tektronix 4010 terminals or Hewlett-Packard* 2647 terminals. Other graphics packages can easily be substituted if the necessary initialization, absolute motion, and absolute vector drawing primitives are available in either software or terminal firmware. If these subroutines are made into dummy subroutines, graphics output will not be available from the program except through the plot output file. The data written into the plot output file, file 2, are a sequence of non-negative x- and y-coordinate pairs. The first line of the file contains the minimum and maximum values of the x- and y-coordinates. Each plot is terminated by a set (or sets) of negative coordinate pairs. The subroutines R1MACH, D1MACH, and I1MACH are used to set machine constants which are used in the other program modules to set machine-dependent quantities. The original versions of the functions are discussed in reference [15] as are the procedures used to calculate these constants for a type of computer which is not presently included. A list of the types of computers which have these constants stored in comment statements, in the existing

* See disclaimer on page 1.

versions of functions, is given in table 1. To convert the program from any of these computer systems to another, the data statements for the old computer are converted to comments, and the C's on the data statements for the new computer are removed.

The conversion of the program from one computer type to another should not require modification of any part of the program which is not in the SYSTEM module. The program was converted from the DEC-20 to the VAX 11/780 in a few minutes of editing time. This assumes that some plotting package is available and that timing subroutines are available on the target computer system.

The module PDESUB.FOR contains the subroutines used to solve the partial differential equations. The theory of these subroutines has been discussed in section 2B above.

The module DEVLIB.FOR contains subroutines used by the other three modules. These subroutines have been obtained from several sources. The error handling software, memory management software, and machine-independent constant software were obtained from [15]. The fast elliptic solver was obtained from [14]. In the initial approximation quadrature from [16] and root finding routines from [17] are used. In the PDESUB module, the Yale Sparse Matrix Package is used [12].

B. Physical Restrictions

Three physical restrictions have been imposed in the present implementation of the CS1 program. First, the two-dimensional electric field dependence of the mobility has not been included. Second, the detailed slopes of the source-and-drain doping profiles have not been included in the model. Third, the work function difference between the gate material and the bulk semiconductor is not included.

The first limitation is the most serious problem. In circuit models and in some two-dimensional device simulation programs, the field dependence of the mobility is empirically included using an expression of the form $a/(1+b \cdot E)$ where a and b are empirically determined parameters and E is the magnitude of the electric field. Recent work by Cooper and Nelson [18] suggests that this model is not adequate to characterize the field dependence of the mobility. On the other hand, the Cooper and Nelson data do not include several effects which are known to affect the low field value of the mobility; these are the effect of bulk doping and oxide interface quality. Since no definitive model for the two-dimensional dependence of the mobility is available, none has been included. Future versions of the program are expected to include such a model.

The details of the two-dimensional source-and-drain profiles are included in the model only as two elliptic abrupt junctions. This allows the details of the majority carrier quasi-Fermi level to be neglected and greatly simplifies the program, making the charge-sheet calculation much more efficient. On the other hand at high source-drain-voltages, this approximation can lead to convergence problems and/or to inaccurate modeling of the potential near the drain. In addition, this model places the burden of specifying lateral and

Table 1. Available Computer Types.

Type	Model	Speed (DEC-20=1)
Burroughs	1700 5700/6700/7700	
CDC	6000/7000	3.3 (Cyber 175)
Cray	1	
Data General	Eclipse S/200	
Harris	220	
Honeywell	600/6000	
IBM	360/370	
Xerox	Sigma 5/7/9	
PDP-10	Ka or Ki	1.0 (K1)
PDP-11		
VAX	11/780	0.72
Univac	1100	0.57 (1108)

Table 2. Transistor Parameters.

Name	Value
Channel Lengths	4.65, 3.20, 1.89, 1.12 μm^*
Vertical Junction Depth	1.05 μm
Lateral Junction Diffusion	0.68 μm
Channel Impurity Density	$1.0 \times 10^{15} \text{ cm}^{-3}$
Source-Drain Impurity Density	$1.0 \times 10^{20} \text{ cm}^{-3}$
Oxide Thickness	51.5 nm
Channel Width	81 μm

* These lengths were obtained from scanning electron microscope measurements of polysilicon length made by P. Roitman.

vertical junction depths on the program user. Other available two-dimensional device simulation programs, such as MINIMOS [4], attempt to include simple two-dimensional process models in the device modeling programs. These simplified models do not agree with more complex two-dimensional models [19] or with experimental measurement of two-dimensional junction shape [20]. If the user of the program wishes to use these simplified models, then the work of Kennedy and O'Brien can be used [21]. If more complicated models [19] or experimental data are available, then these can be used.

The least serious of the restrictions is that the work function difference between the gate material and the bulk semiconductor is not included. This difference, if it is known, can be included in the gate bias.

4. Device Model Verification

This section is divided into three parts. In the first part, the numerical accuracy of the model is evaluated. In the second part, the one- and two-dimensional models are compared for a transistor similar to the transistor studied by Brews [2]. In the third part, experimentally measured data are compared to the one- and two-dimensional models. The transistors used in this experimental study were taken from an array of transistors fabricated using an SEM-compatible transistor array of the type discussed in reference [22]. This pattern has been incorporated into test pattern NBS-28A [22]. In this study the polysilicon gate lengths were measured using a scanning electron microscope, and the metallurgical channel lengths were obtained using estimates of lateral-to-vertical arsenic diffusion in reference [19]. The relevant device simulation parameters are given in table 2. The heavily doped source-and-drain regions are excluded from the region of calculation because the potential in the regions is pinned to the source or drain potential plus the built-in potential, and the ratio of channel to source-drain depletion depth is more than 100 to 1.

The numerical accuracy of two different adaptive meshing procedures is discussed. The first procedure, referred to as the direct method, uses adaptive mesh generation to refine the mesh. After each adaptation, the resulting linear equations are solved by direct methods. Multigrid iteration is not used. The second method, referred to as the multigrid method, uses adaptive mesh generation to obtain a sequence of more refined mesh levels. A multi-level iteration over these levels is then used for the solution of the linear equations.

The problem used as a test case for numerical accuracy studies is a 1.12- μm n-channel transistor with 0.2 V of applied source-drain voltage and a gate voltage 0.7 V above threshold. This transistor, under these bias conditions, carries a drain current of 88 μA . The level 2 mesh and a contour plot of the electrostatic potential for this calculation are shown in figures 2a and 2b. The progress of the iteration process for this simulation, using the direct method, is given in table 3. In this case, and all other convergent cases, the direct and multigrid methods yield similar accuracies for the specified number of level 1 and level 2 iterations. The direct method is more robust and has converged in cases where the multigrid method fails.

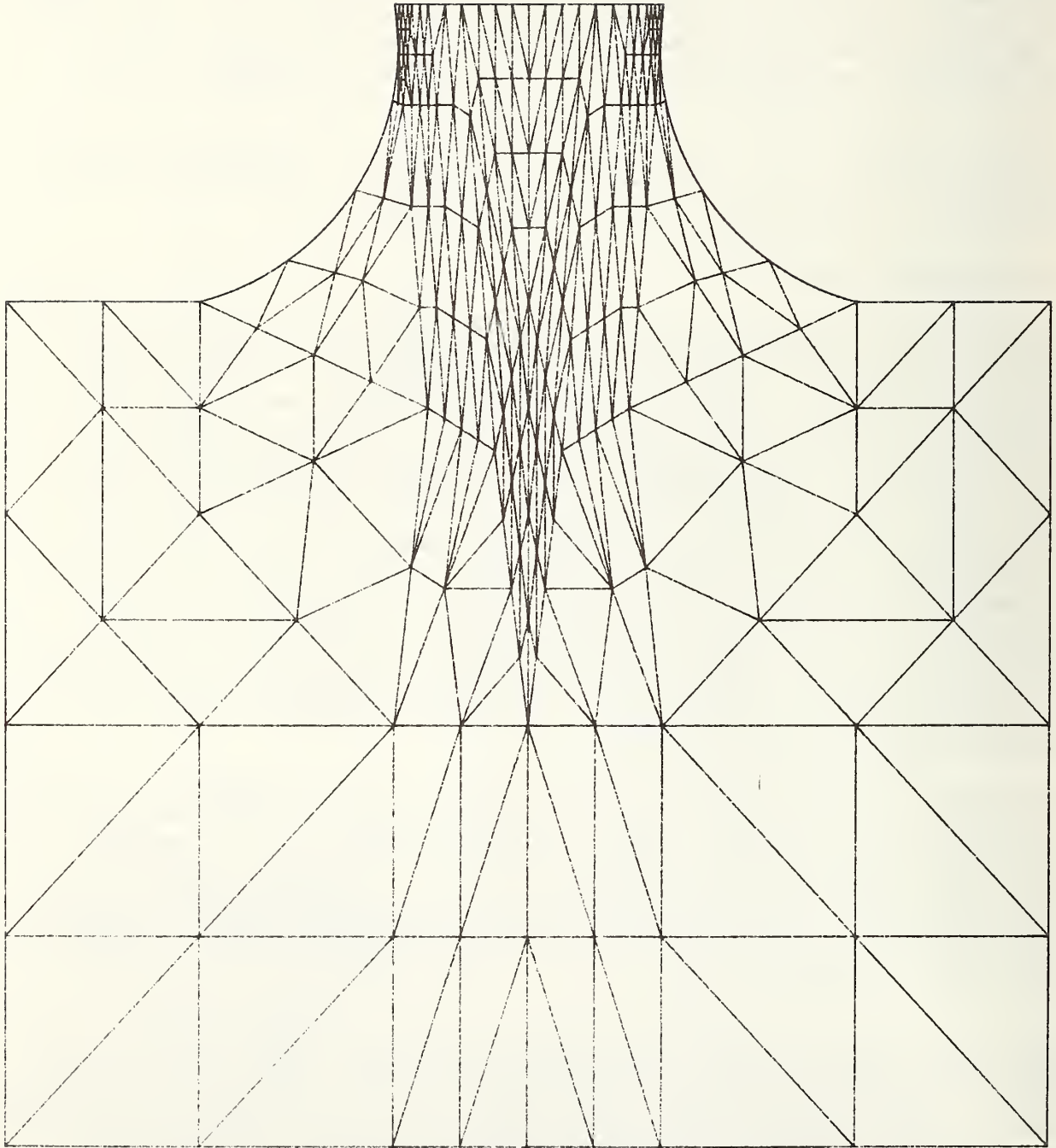


Figure 2. a) Two-dimensional level 2 mesh for the 1.12- μm transistor.

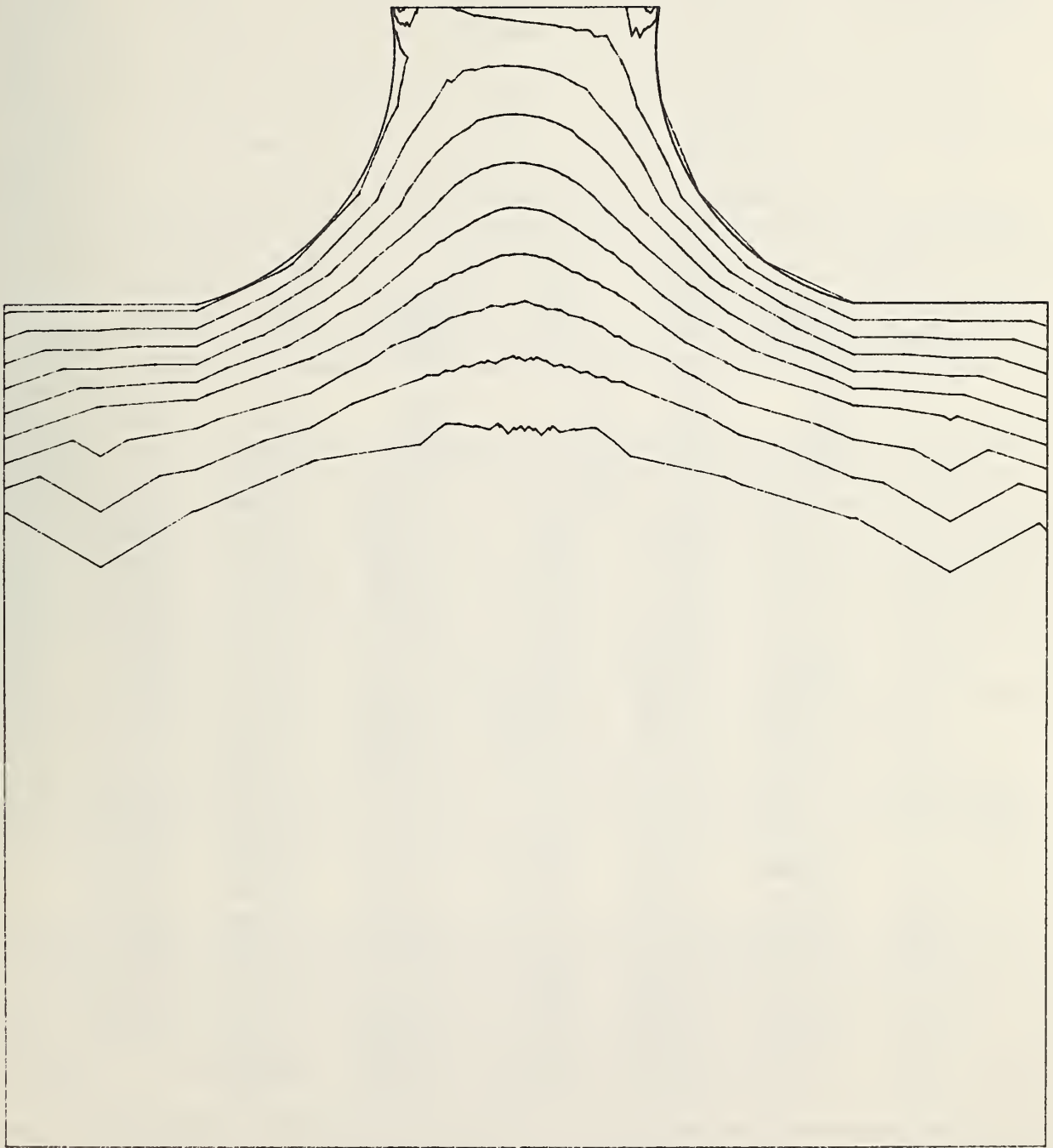


Figure 2. b) Two-dimensional equipotentials for the 1.12- μm transistor.

Table 3. Iteration Convergence.

Iteration	Level 1			Level 2		
	Newton norm	$\Delta\psi_s$	ΔJ_s	Newton norm	$\Delta\psi_s$	ΔJ_s
1	36.1	3.31	771	24.9	3.78	0.36
2	14.6	1.28	634	24.9	3.70	0.34
3	7.24	1.25	340	3.63	0.809	0.87
4	7.22	1.25	146	0.798	0.679	0.37
5	2.14	1.24	59.9	0.653	0.556	0.31
6	1.78	1.22	23.7	0.548	0.488	0.30
7	1.22	1.19	8.8	0.488	0.473	0.29
8	1.15	1.13	3.01	0.462	0.447	0.26
9	1.05	1.03	1.01	0.431	0.416	0.23
10	0.94	0.91	0.53	0.398	0.385	0.21
11	0.829	0.803	0.43	0.365	0.353	0.18
12	0.722	0.698	0.36	0.333	0.323	0.16
13	0.624	0.602	0.28	0.304	0.294	0.14
14	0.537	0.510	0.22	0.276	0.268	0.12
15	0.459	0.442	0.17	0.250	0.244	0.11
16	0.392	0.377	0.14	0.227	0.221	0.09
17	0.334	0.322	0.11	0.205	0.200	0.08
18	0.285	0.274	0.08	0.186	0.181	0.07
19	0.233	0.242	0.07	0.168	0.164	0.06
20	0.207	0.199	0.05	0.152	0.148	0.04
21	0.176	0.169	0.03	0.137	0.134	0.03
22	0.150	0.144	0.03	0.124	0.122	0.02
23	0.127	0.123	0.02	0.113	0.113	0.02
24	0.108	0.104	0.01	0.104	0.103	0.01
25	0.092	0.089	0.01	0.094	0.095	
26	0.076	0.078		0.088	0.087	

The convergence of each iteration is evaluated by plotting the average Newton step size (Newton norm) as a function of the iteration number. These data are shown for the direct case in figure 3. The corresponding multigrid case is shown in figure 4. In each case the convergence sequence is divided into two regions. For the first few iterations, the Newton norm falls rapidly from a very inaccurate initial value to a value of approximately 1, in normalized units, or approximately 0.026 V. The convergence then proceeds linearly, at a slower uniform rate, until the convergence criterion is reached or the maximum allowed iteration count is exceeded. As the number of mesh points is increased, by increasing the level of the mesh, the convergence rate decreases; it takes more iterations to reduce the Newton norm to some specified value. The reduced rate of convergence is the result of the approximate Jacobian in eq (26) used in eq (22). The smallest Newton norm is obtained with the level 2 mesh after 23 iterations. Solutions obtained with other channel lengths and bias voltages using different numbers of quadrature points for the solution of eq (11) and different oxide mesh densities show, in all cases, that the optimal solution is obtained using the level 2 mesh.

Although the error evaluation technique discussed above provides an accurate measure of the convergence of the numerical method, two other error evaluation techniques are also useful. In one method, the maximum change in the surface potential at the semiconductor-oxide interface after each Newton step is compared to the Newton norm of that step. A graph of this relationship is shown in figure 5. In the initial iterations of each convergence sequence, the Newton norm falls rapidly, while only minimal improvement in the surface potential is made. As the Newton norm approaches 1.0, the values of $\Delta\psi_s$ and the norm become identical. Again, the iteration is divided into two parts. In the first part, the two-dimensional potential is refined, and the surface potential is only crudely calculated. This process converges rapidly. The second part of the process is dominated by successive refinements of $\Delta\psi_s$, and the two-dimensional potential is dominated by surface potential boundary effects. The level 3 iteration divergence occurs because the Jacobian in eq (26) is not sufficiently exact to allow the Newton method to converge for the multigrid solution of the linear equations.

The most important error estimation method compares $\Delta\psi_s$ to ΔJ_d , the difference in the drain current between the value at the present iteration and the final value of the drain current. These data are plotted for the test problem in figures 6a and 6b for both level 1 and level 2. In the level 1 case, the value of ΔJ_d falls slowly as $\Delta\psi_s$ decreases from 30 to 2. As $\Delta\psi_s$ decreases from 2 to 1, the current convergence is very rapid. Finally, if $\Delta\psi_s < 1$, the current converges quadratically with $\Delta\psi_s$.

Only the quadratic region of convergence is important for the level 2 case shown in figure 6b. The initial error in the first region is represented by two points near $\Delta\psi_s = 3$, and no structure is visible. The relationship of ΔJ_d and $\Delta\psi_s$ to the Newton norm is important in that it allows the convergence of the equation solution process to be monitored by the Newton norm. For small Newton norms, less than one, the approximation $\Delta J_d = \text{constant} (\text{Norm})^{1/2}$ is valid. A request for a 0.1 Newton norm (i.e., 0.1 kT/q) allows the error in the current to be reduced to 0.16 percent and a 0.4 Newton norm produces a 1.6-percent error.

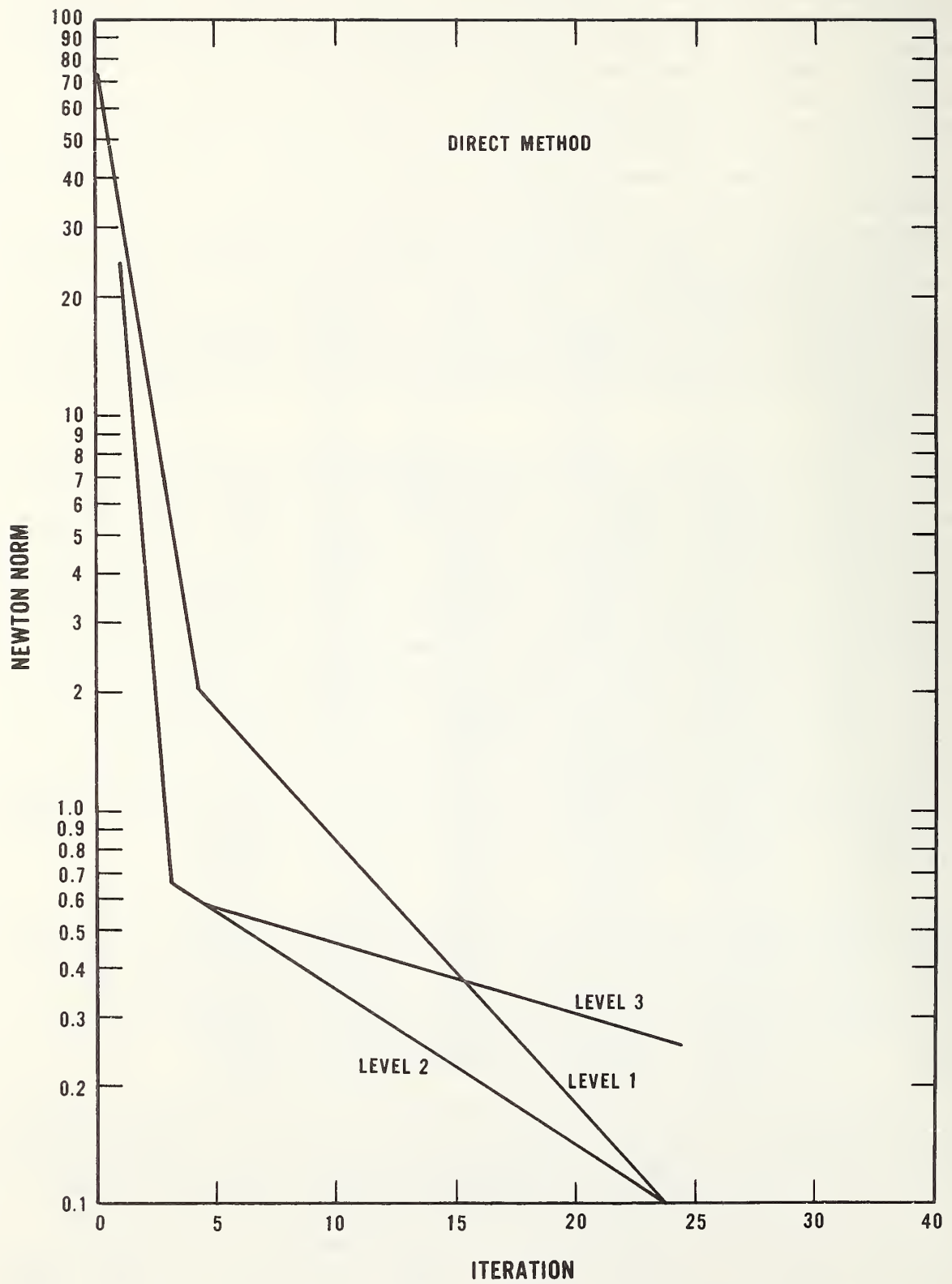


Figure 3. Convergence of the direct method for the test problem.

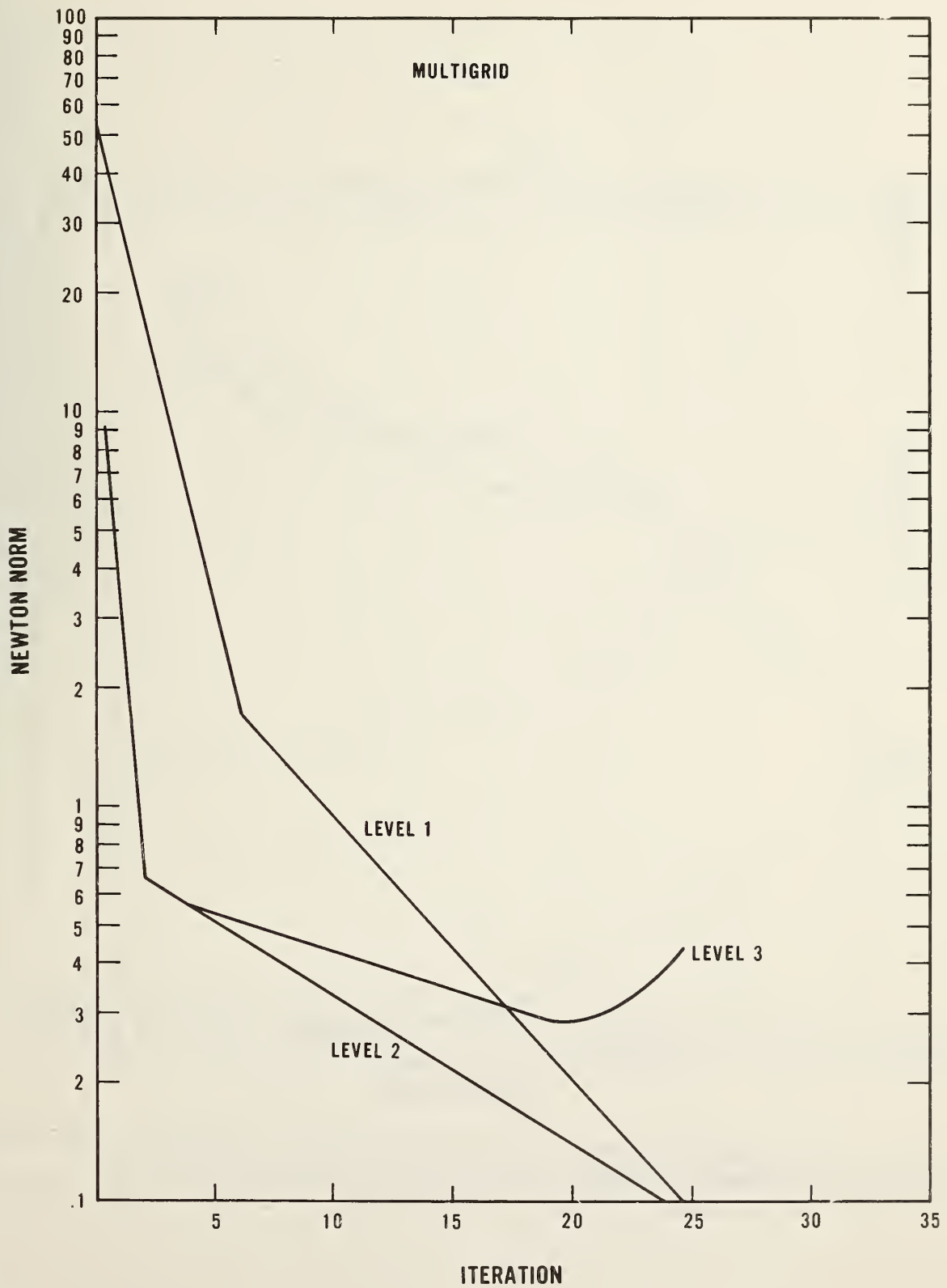


Figure 4. Convergence of the multigrid method for the test problem.

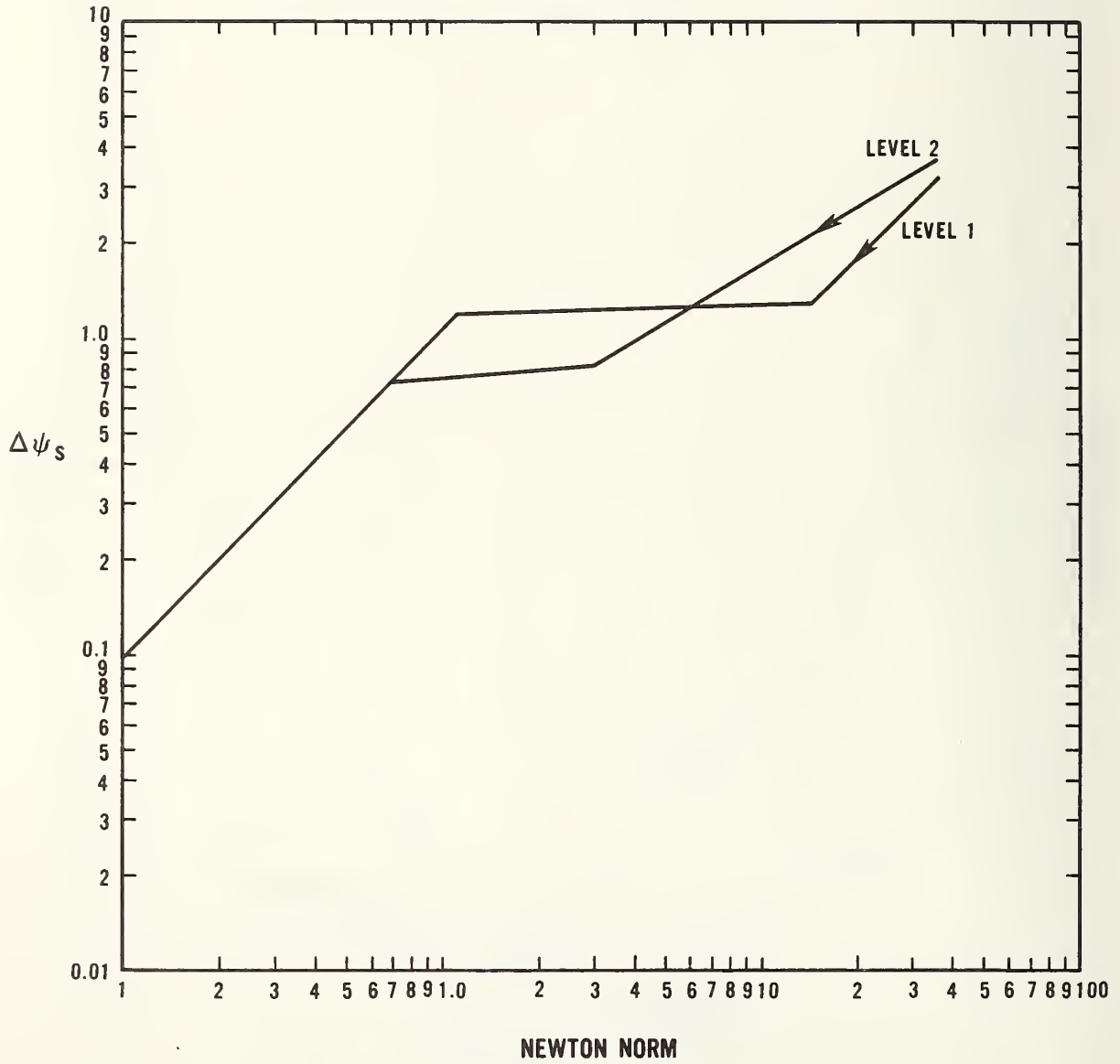


Figure 5. Relationship between the surface potential change and the Newton step size for the test problem.

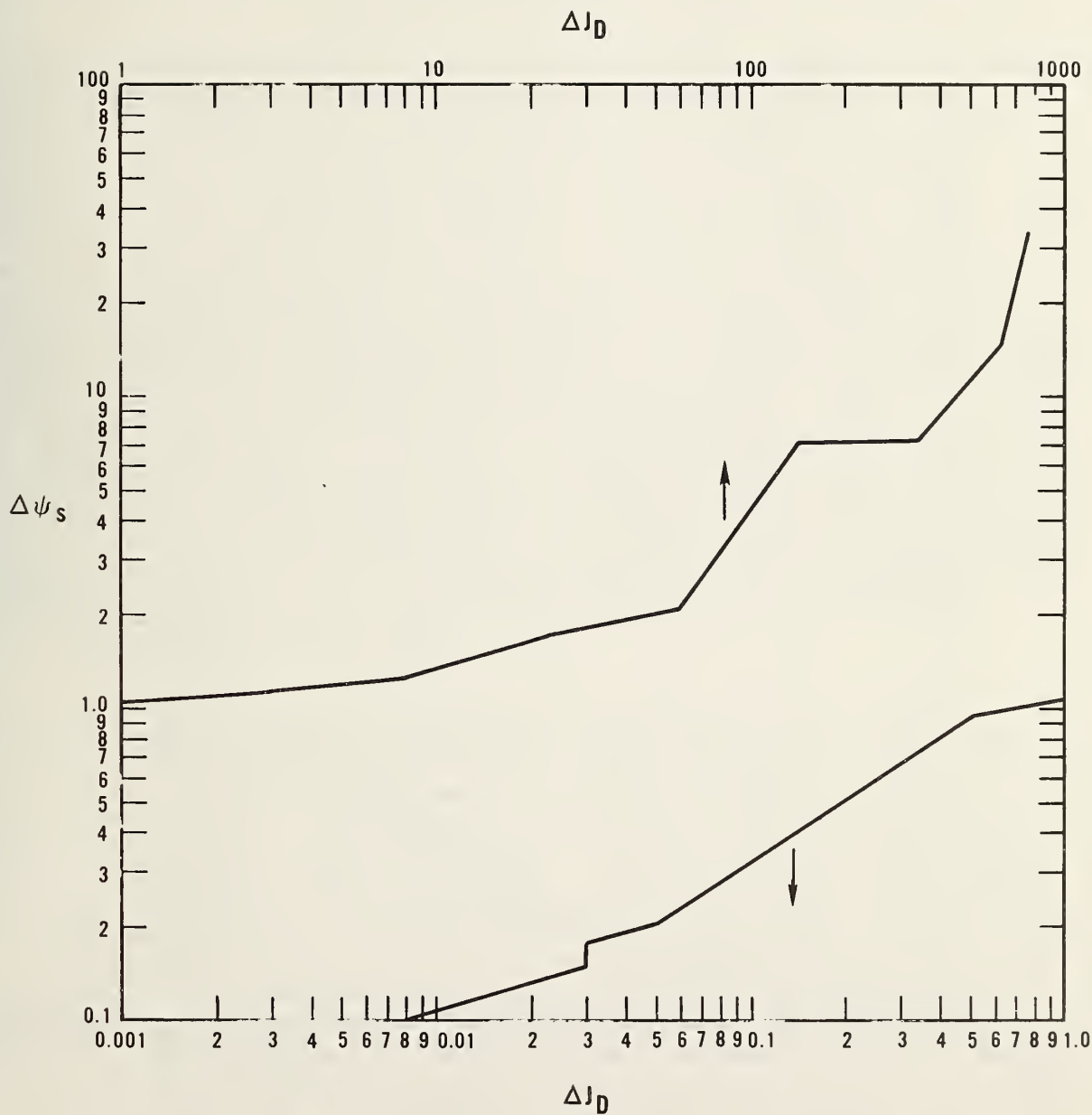


Figure 6. a) Relationship between surface potential change (kT/q) and drain current change (arbitrary unit, $J_D = 1$) for the level 1 mesh.

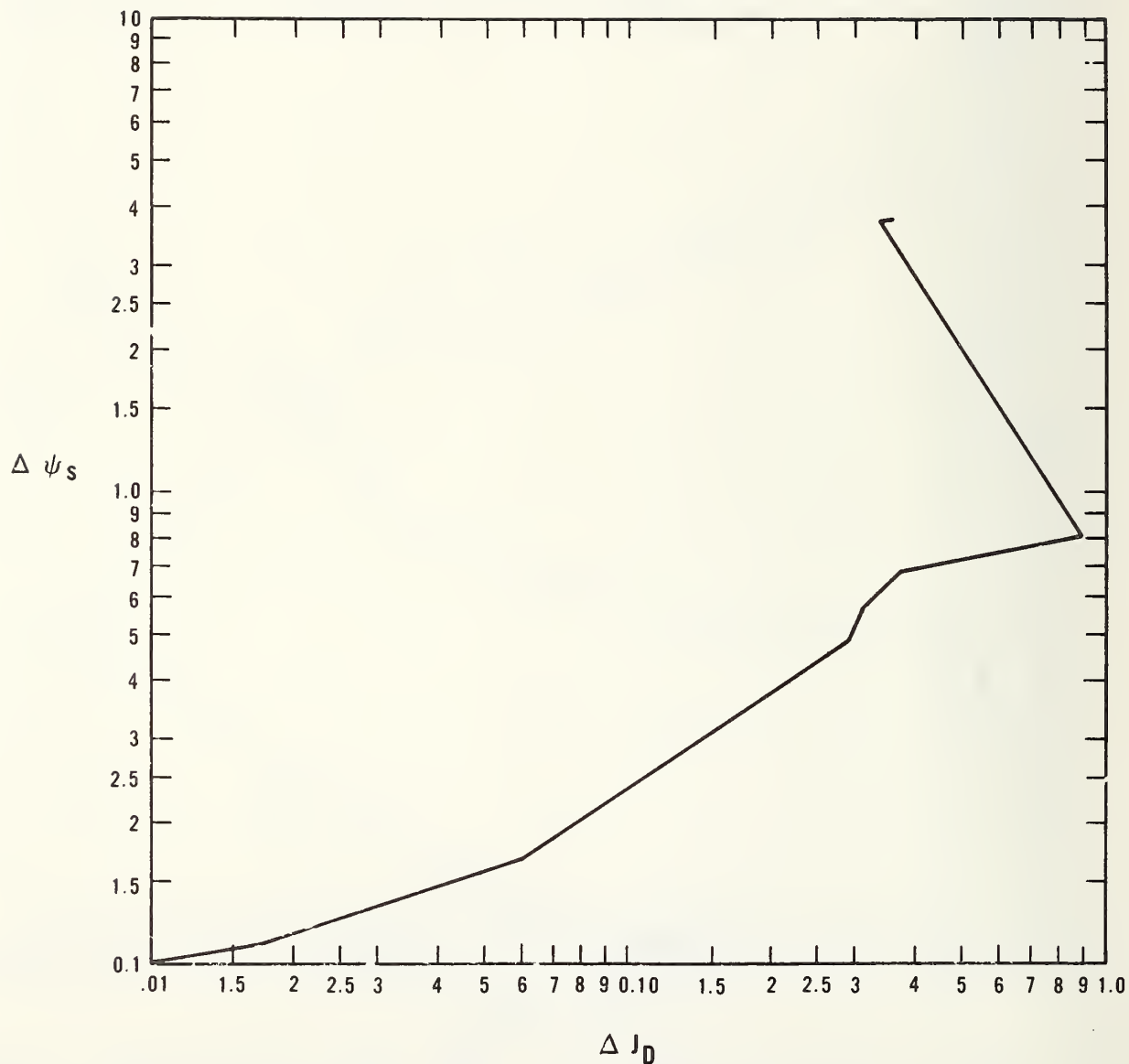


Figure 6. b) Relationship between surface potential change (kT/q) and drain current change (arbitrary unit, $J_D = 1$) for the level 2 mesh.

From this discussion of numerical accuracy, one can conclude that the accuracy of this implementation of the charge-sheet model can greatly exceed the accuracy required for most applications. To obtain 5-percent accuracy for drain current, a level 1 mesh using 10 Newton steps and a relative Newton step convergence criterion of 2 percent are sufficient. Refinement of the level 1 mesh to level 2 gives a J_d which is more accurate than required.

Next, the difference between the one- and two-dimensional charge-sheet model in their long-channel limit is discussed. A transistor similar to the transistor shown in figure 5 of Brews' paper [2] is considered. The substrate doping is 10^{15} cm^{-3} , the oxide thickness is 100 nm, and for the two-dimensional case the polysilicon length is $4.6 \mu\text{m}$, with $0.3 \mu\text{m}$ of lateral junction diffusion at each edge, and $0.5 \mu\text{m}$ of vertical junction depth. The one-dimensional theory used here is Brews' eq (11); no simplifications have been made. The results of these one- and two-dimensional calculations are shown in figure 7. Although the transistor is a short-channel transistor in the sense discussed in reference [9], no threshold voltage offset or change in output conductance in the saturation region is calculated. The two calculations are in good agreement throughout the region shown. Similar agreement has been obtained for a transistor with $8.6\text{-}\mu\text{m}$ polysilicon, 50-nm gate oxide, and substrate doping of $5 \times 10^{14} \text{ cm}^{-3}$. In the long-channel limit, the one- and two-dimensional charge-sheet models are in good agreement. If the characteristics of the device being modeled are not dominated by short-channel effects in the triode and saturation regions, the one-dimensional charge-sheet model provides an adequate model of the transistor well below the limit discussed in reference [9]. This is true since the effects studied in [9] for subthreshold regions are not associated with large current changes in other regions of device operation.

The two-dimensional charge-sheet model can be used to characterize MOS transistors in regions where both threshold voltage offset and variable output conductance are important. In the triode region of operation, as the channel length of the transistor is decreased, the two-dimensional electrostatic fields associated with the source-and-drain junctions extend significantly into the channel region and cause surface inversion, even when the gate potential is substantially below threshold. This is an electrostatic effect and is well modeled by the two-dimensional charge-sheet model. This region of transistor operation is shown in figure 8 for transistors with 4.65- , 3.2- , and $1.12\text{-}\mu\text{m}$ channel lengths. For the $4.65\text{-}\mu\text{m}$ transistor, both one- and two-dimensional theories are adequate to model the triode region and the high current part of the subthreshold region shown in figure 8. For the $3.2\text{-}\mu\text{m}$ transistor, the two-dimensional model is in good agreement with the measured data, while the one-dimensional model is diverging from these data. For the $1.12\text{-}\mu\text{m}$ transistor, the two-dimensional model shows a threshold voltage offset of 0.060 V. This threshold voltage offset results in a 26-percent increase in measured current, as compared to the one-dimensional model, when the gate voltage is 0.25 V. At some channel length below $1.0 \mu\text{m}$, these two-dimensional electrostatic effects will become so large that the channel current will no longer be confined to the surface of the transistor and the charge-sheet model will fail. This is not the case for the short-channel transistors modeled here.

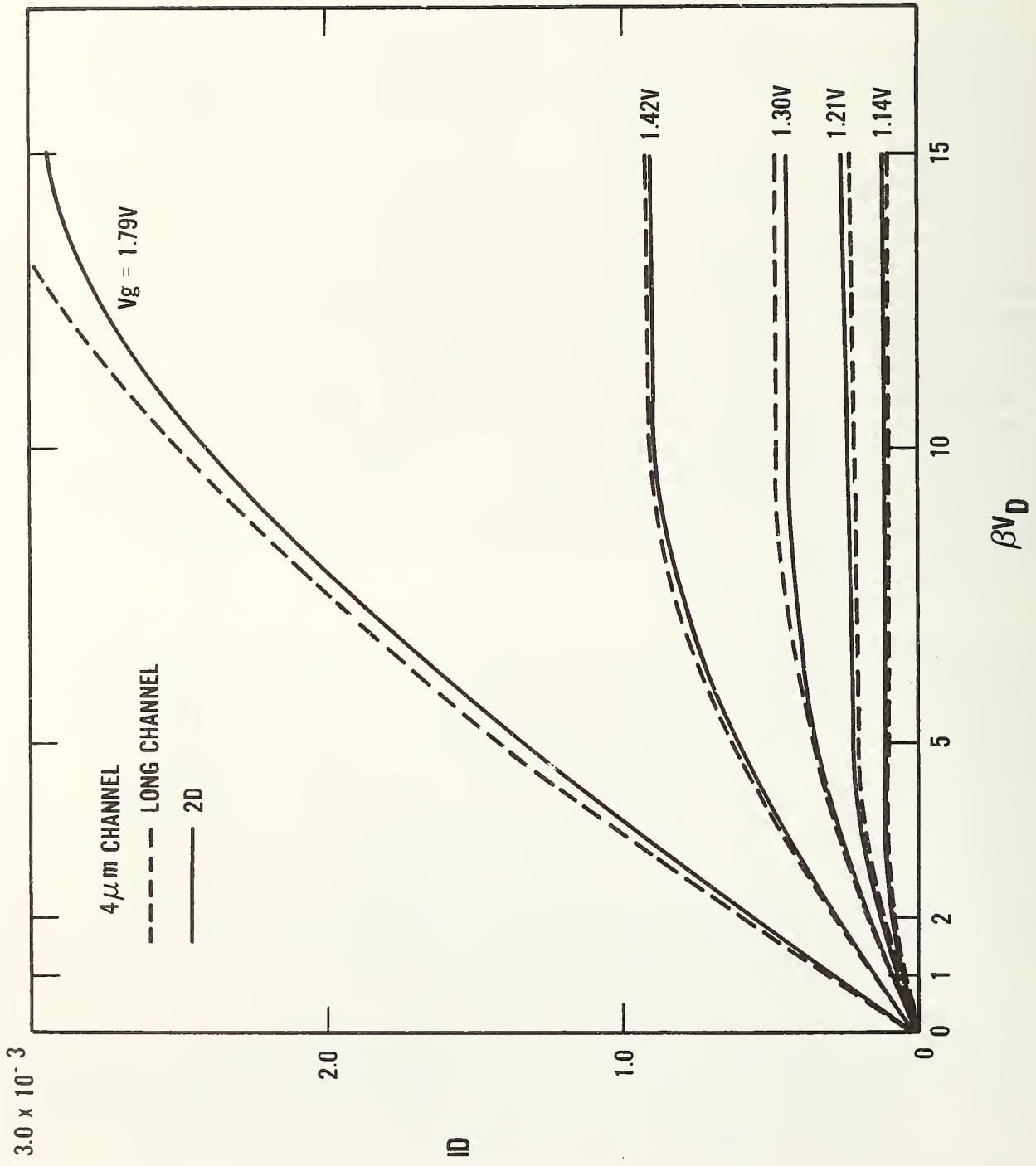


Figure 7. Comparison of the drain current calculated by the one- and two-dimensional models.

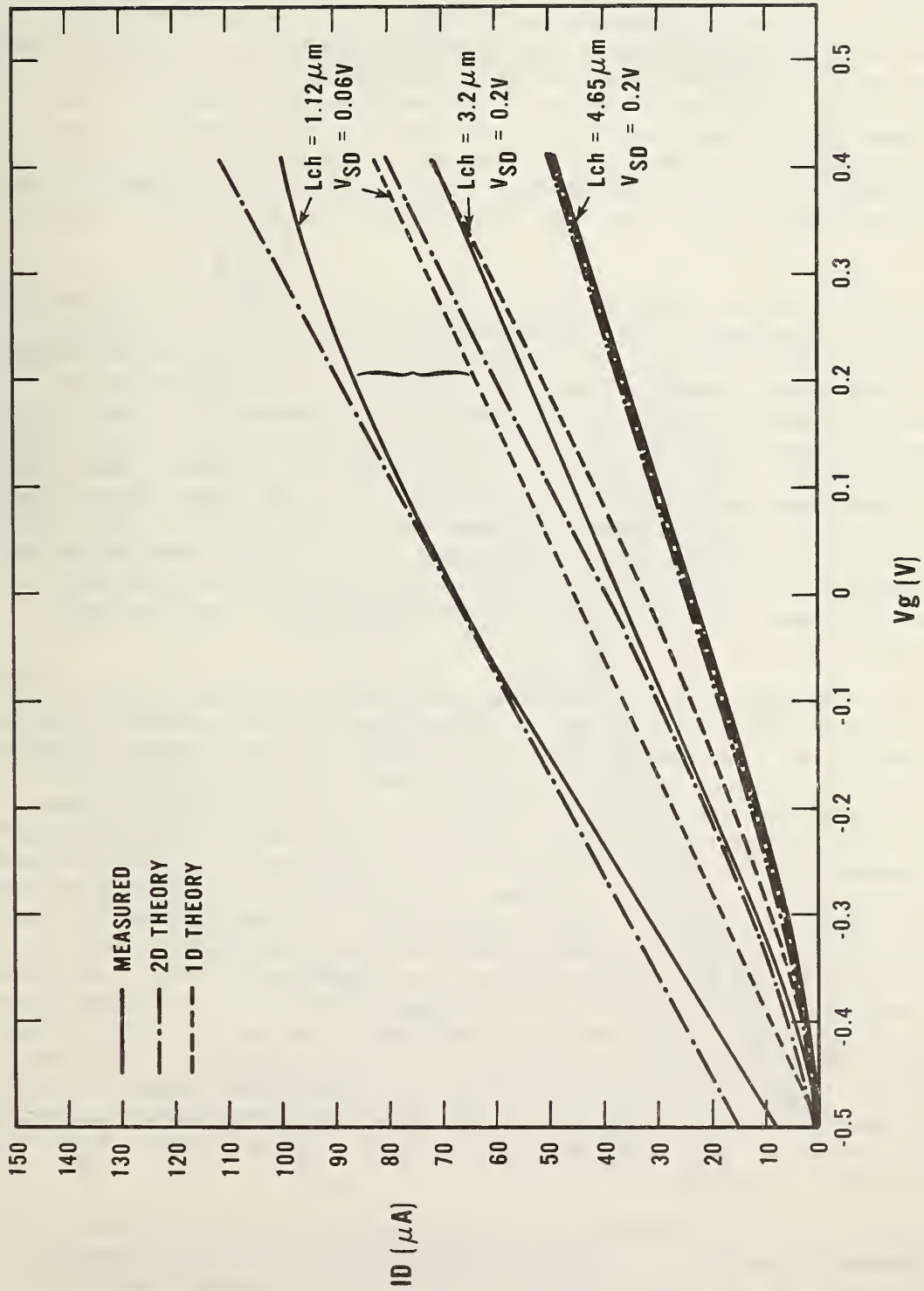


Figure 8. Comparison of the subthreshold and triode region drain current measured and calculated using the one- and two-dimensional models.

As the source-drain voltage is increased, the apparent threshold voltage offset produced by two-dimensional electrostatics is increased, along with the size of the depletion region around the drain. This effect is shown in figure 9 for a source-drain voltage of 0.5 V; four transistors are shown with 1.12-, 1.89-, 3.20- and 4.65- μm channel lengths. In the shortest channel transistor, at 0.25-V gate voltage the measured drain current is twice the value given by the one-dimensional theory. Agreement with the two-dimensional model is within 3 percent. For the 1.89- μm transistor, the agreement with two-dimensional theory is within 5 percent; at 0.25-V gate voltage, the measured current is 1.5 times the current given by the one-dimensional model. For the long-channel lengths, the measured data and the two-dimensional model both agree with long-channel theory to better than 1 percent.

In the saturation region, neither of the charge-sheet models is satisfactory for the 1.12- μm transistor. The two-dimensional model does not converge, because field reversal effects in the channel occur along the entire channel length. As the source-drain voltage is increased, the depletion region around the drain expands under the channel. This expanded drain depletion region causes current flow away from the surface channel and, at some voltage below punch-through, causes the field in the channel to reverse. This field reversal effect shortens the effective channel length and draws charge away from the semiconductor-oxide surface charge sheet. The effect of this distributed charge is not adequately represented in the charge-sheet model and leads to convergence problems in the saturation region of the transistor. This effect decreases with increasing channel doping and would not occur until 0.5 μm if channel doping were $1 \times 10^{16} \text{ cm}^{-3}$.

Although some convergence problems occur due to field reversal in the channel, it is possible to make useful comparisons between measured data and the two-dimensional charge-sheet model for transistors with channel lengths longer than 1.12 μm . The transition between output characteristics which look like long-channel characteristics in the saturation region and those which look like short-channel characteristics occurs between 3.20- μm and 1.89- μm channel lengths. The model results are compared for these two cases in figures 10 and 11. In figure 11a the 1.89- μm transistor model is compared to measured data. In figure 11b the experimental data are compared to the long-channel theory of the one-dimensional charge-sheet model. There is no similarity between the long-channel theory and the measured data. The long-channel theory fails because the effect of source-drain field-induced channel inversion is neglected. This channel inversion is dominated by the source-drain field, since the calculated threshold voltage offset for this transistor, shown in figure 8, is not large enough to explain this change in drain current. The source-drain component of the field produces such an offset, as is shown in figure 9. The additional source-drain-induced offset dominates the effect shown in figure 11.

Two interesting physical effects are also observed in the calculation of the 1.89- μm channel transistor. In the saturation region of the transistor, a significant part of the total channel is in the field reversal region. If the charge associated with this field reversal region is removed from the calculation of eqs (11) and (12), good agreement between the model and the experimental data is obtained as shown in figure 11a. This observation also

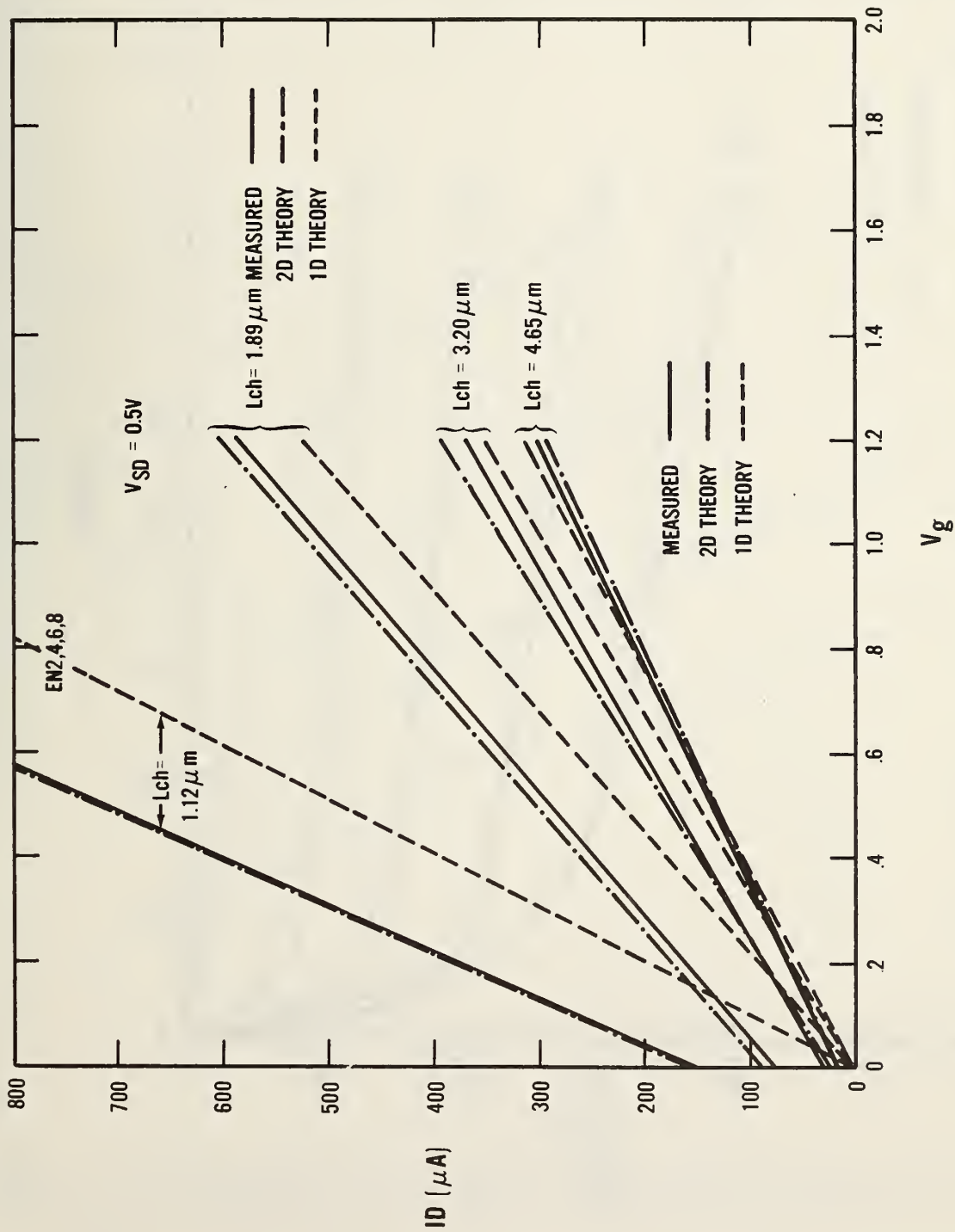


Figure 9. Comparison of the triode region drain current measured and calculated using the one- and two-dimensional models.

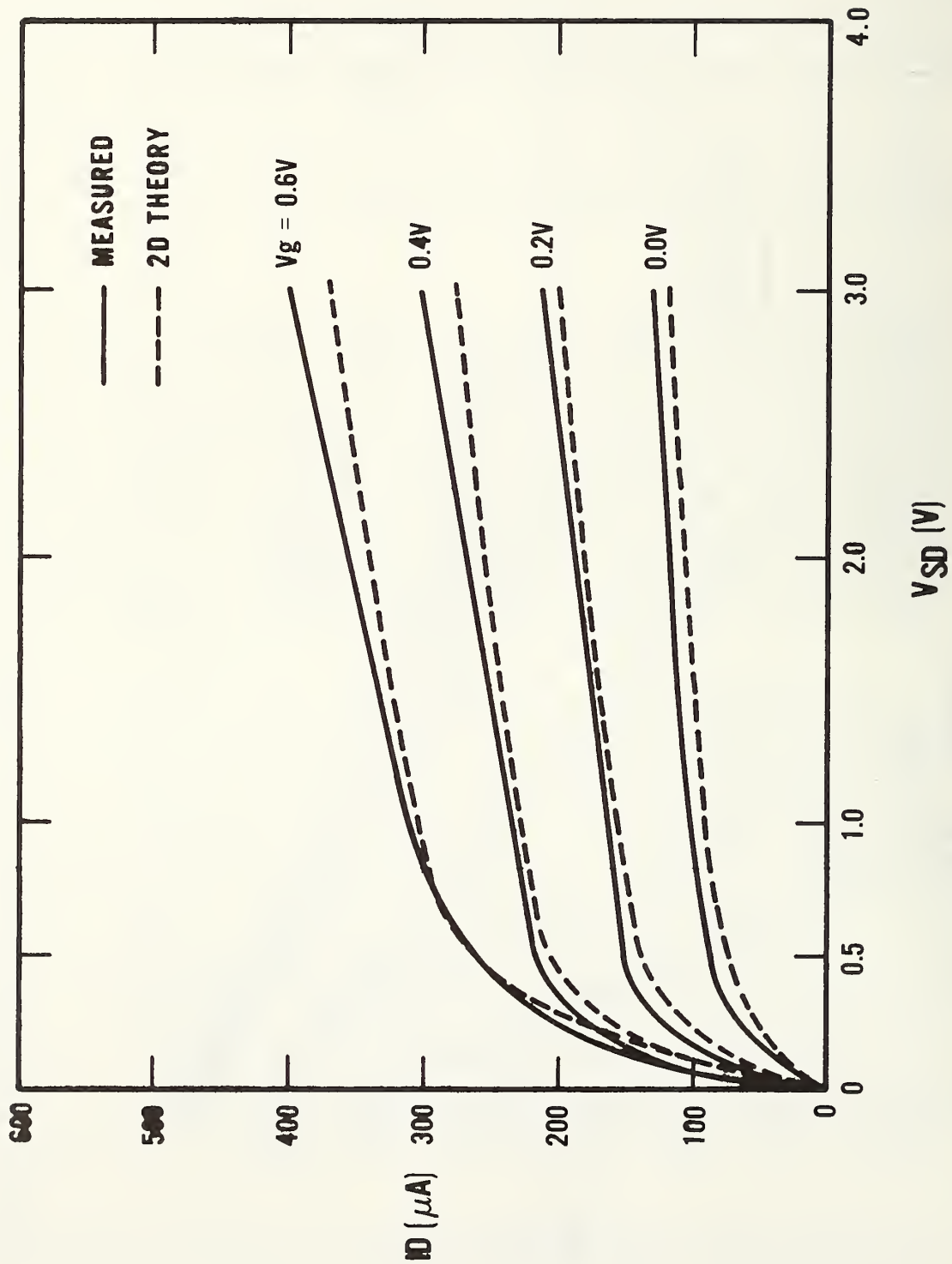


Figure 10. Comparison of the output characteristics measured and calculated using the two-dimensional model for the $3.20\text{-}\mu\text{m}$ transistor.

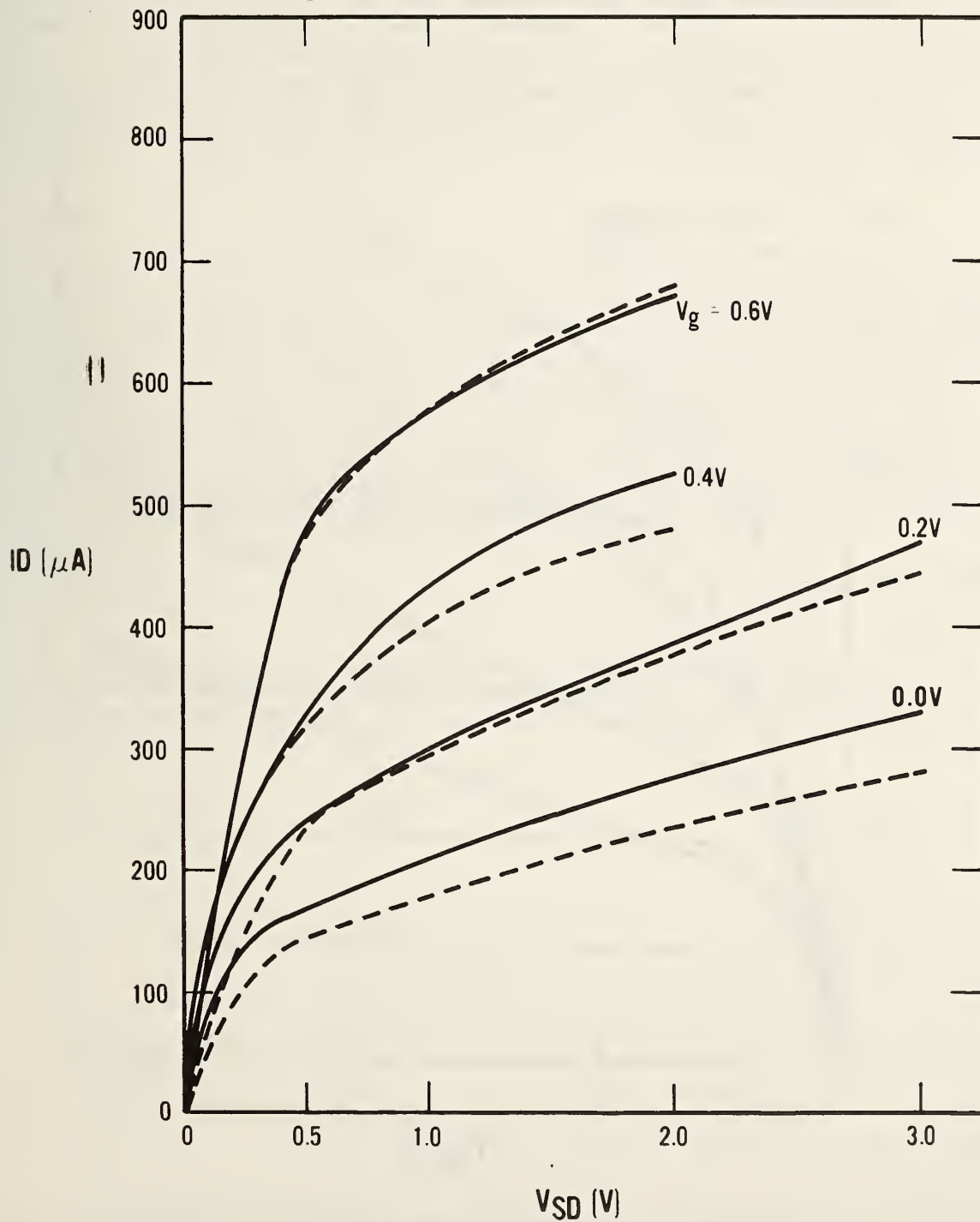


Figure 11. a) Comparison of the output characteristics measured and calculated using the two-dimensional model for a 1.89- μm transistor.

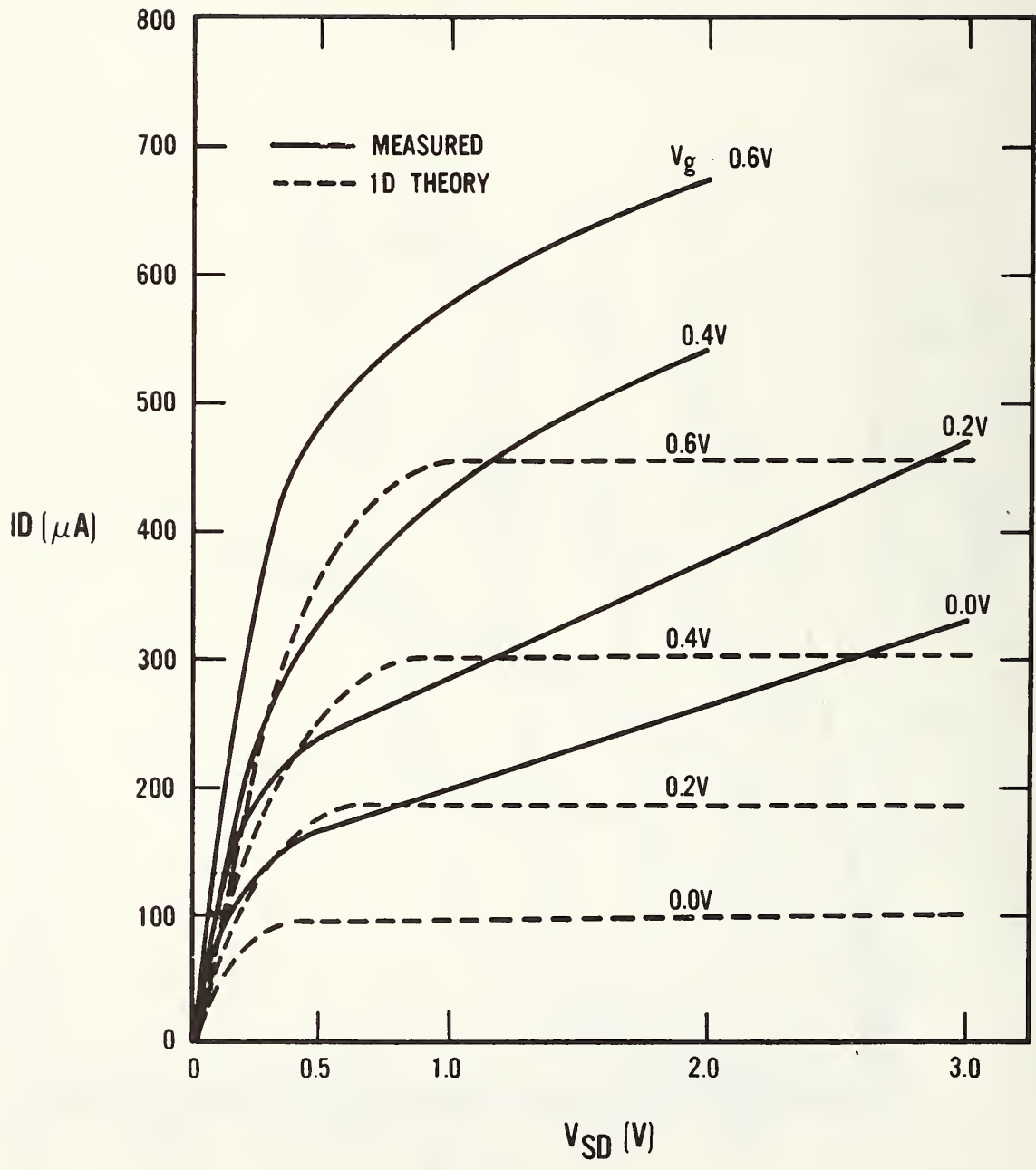


Figure 11. b) Comparison of the output characteristics measured and calculated using the one-dimensional model for a 1.89- μm transistor.

explains the modulation of the output conductance in figure 11a without the inclusion of field dependent mobility. The effective decrease in conductivity occurs because the part of the channel which is not experiencing field inversion is constrained by strong electrostatic effects originating in the drain. In the transition region between the triode and saturation regions in figure 11b, the long-channel theory, with the same mobility, overestimates the drain current. Strong two-dimensional electrostatic effects at low source-drain voltages slow the process of channel inversion and at higher source-drain voltages enhance it, shortening the channel by field inversion.

5. Conclusions

A two-dimensional charge-sheet model of a surface-channel MOS transistor has been developed. When this model is implemented using adaptive finite element methods, an efficient high-accuracy transistor simulation program is possible. The simulations produced using this model have been compared to experimental measurements; the model is in good agreement for transistors with channel lengths as short as $1.12 \mu\text{m}$. In this verification process the model represented accurately the onset of subthreshold current, channel-length-induced threshold voltage offset, and drain-field-induced output conductance changes. These drain-field-induced output conductance changes are successfully modeled by constant channel mobility and do not require use of high field mobility effects.

Acknowledgments

The authors wish to thank C. W. Gwyn for providing computer support for this work, E. H. Nicollian for providing the experimental transistors, J. R. Brews for helpful discussion of his charge-sheet model, and P. Roitman for SEM measurements.

References

1. De La Moneda, F., Threshold Voltage from Numerical Solutions of the Two-Dimensional MOS Transistor, *IEEE Trans. Circuit Theory* CT-20, 666-673 (1973).
2. Brews, J. R., A Charge-Sheet Model of the MOSFET, *Solid-State Electronics* 21, 345-355 (1978).
3. Greenfield, J. A., and Dutton, R. W., Nonplanar VLSI Device Analysis Using the Solution of Poissons's Equation, *IEEE Trans. Electron Devices* ED-27, 1520-1532 (1980).
4. Selberherr, S., Schutz, A., and Potzl, H. W., MINIMOS - A Two-Dimensional MOS Transistor Analyzer, *IEEE Trans. Electron Devices* ED-27, 1540-1549 (1980).
5. Buturla, E. M., and Cottrell, P. E., Two-Dimensional Finite-Element Analysis of Semiconductor Steady-State Transport Equations, *Int. Conf. on Computational Methods in Nonlinear Mechanics*, Austin, Texas, 1974.
6. Fichtner, W., and Rose, D. J., On the Numerical Solution of Nonlinear Elliptic PDE's Arising from Semiconductor Device Modeling, *Elliptic Problem Solvers*, M. Schultz, Ed. (Academic Press, New York, 1981), pp. 277-284.
7. Bank, R. E., and Sherman, A. H., PLTMG User's Guide, CNA-152, Center for Numerical Analysis, University of Texas at Austin, September 1979.
8. Laux, S. E., and Lomax, R. I., Numerical Investigation of Mesh Size Convergence Rate of Finite Element Method in MESFET Simulation, *Solid-State Electronics* 24, 485-493 (1981).
9. Brews, J. R., Fichtner, W., Nicollian, E. H., and Sze, S. M., Generalized Guide for MOSFET Miniaturization, *Electron Device Letters* EDL-1, 2-4 (1980).
10. Wilson, C. L., and Blue, J. L., Semiconductor Device Simulation, *Elliptic Problem Solvers*, M. Schultz, Ed. (Academic Press, New York, 1981), pp. 435-439.
11. Strang, G., and Fix, G. J., *An Analysis of the Finite Element Method* (Prentice-Hall, Englewood Cliffs, N.J., 1973).
12. Eisenstat, S. C., Gursky, M. C., Schultz, M. A. and Sherman, A. H., Yale Sparse Matrix Package I. The Symmetric Codes, Research Report #112, Department of Computer Science, Yale University, 1976.
13. Brandt, A., Multi-Level Adaptive Solutions to Boundary-Value Problems, *Math. Comp.* 31, 333-390 (1977).

14. Swarztrauber, P., and Sweet, R., Efficient FORTRAN Subprograms for the Solution of Elliptic Partial Differential Equations, NCAR Technical Note, NCAR-TN/IA-109, 1975.
15. Fox, P. A., Hall, A. D., and Schryer, N. L., The PORT Mathematical Subroutine Library, *ACM Trans. Mathematical Software* 2, 104-126 (1978).
16. Blue, J. L., Automatic Numerical Quadrature - DQUAD, Bell Labs Comput. Sci. Tech. Rep. 25, February 1975; also, Automatic Numerical Quadrature, *Bell Syst. Tech. J.* 59, 1651-1678 (1977).
17. Brent, R. P., *Algorithms for Minimization Without Derivatives* (Prentice-Hall, Englewood Cliffs, N.J., 1973), pp. 188-189.
18. Cooper, J. A., Jr., and Nelson, D. F., Measurement of High-Field Drift Velocity of Electrons in Inversion Layers on Silicon, *IEEE Electron Device Letters* EDL-2, 171-173 (1981).
19. Warner, D. D., and Wilson, C. L., Two-Dimensional Concentration Dependent Diffusion, *Bell Syst. Tech. J.* 59, 1-41 (1980).
20. Wilson, C. L., Scanning Electron Microscope Measurements on Short Channel MOS Transistors, *Solid-State Electronics* 23, 345-356 (1980).
21. Kennedy, D. P., and O'Brien, R. R., Analysis of the Impurity Atom Distribution Near the Diffusion Mask for a Planar p-n Junction, *IBM J. Res. Dev.* 9, 179-186 (1965).
22. Mitchell, M. A., and Linholm, L. W., *Semiconductor Measurement Technology: Test Patterns NBS-28 and NBS-28A: Random Fault Interconnect Step Coverage and Other Structures*, NBS Spec. Publ. 400-65 (March 1981).

Appendix A
Channel Current Calculation

Following the general method presented by Brews [2], a vertical average (along the x-direction) of the electron quasi-Fermi level is calculated over the channel. The channel charge is then given by:

$$N(y) = n_i e^{-\beta \bar{\phi}_n(y)} \int_0^\infty dx (e^{\beta \phi_{-1}}) = \frac{z f n_i}{\mu^*} \quad (\text{A-1})$$

$$z = e^{-\beta \bar{\phi}_n}, \quad f = \int_0^\infty dx (e^{\beta \phi_{-1}}) \mu_n .$$

This follows from eq (2) and the arguments presented in reference [2]. The integral form of eq (7) then yields:

$$\nabla \cdot \mathbf{J} = 0 = \frac{\partial}{\partial y} \left\{ N(y) \mu^* \frac{d\phi_n(y)}{dy} \right\} \quad (\text{A-2})$$

which can be rewritten as:

$$\frac{\partial}{\partial y} \left(f \frac{dz}{dy} \right) = 0 . \quad (\text{A-3})$$

This equation has the solution

$$z = z_0 + \int_0^y \frac{dy_0}{f(y_0)} . \quad (\text{A-4})$$

Since the total change in the quasi-Fermi level must equal the source-drain voltage drop, for potentials relative to the source:

$$z_0 = 1 \quad A = \frac{e^{-\beta V_d - 1}}{\int_0^L \frac{dy_0}{f(y_0)}} . \quad (\text{A-5})$$

Substitution of these factors into (A-1) yields eq (11). The current is then given by:

$$\mathbf{J} = - \frac{q N_i}{\beta} \mathbf{A} , \quad (\text{A-6})$$

which reduces to eq (12).

Appendix B
File CS1.HLP

1. Interactive Execution

The program is executed by entering:

```
RUN CS1.EXE
```

A prompt will appear for the next input; enter a file name after each prompt, followed by a carriage return (denoted <cr>)

```
FILENAME1<cr>  
FILENAME2<cr>  
FILENAME3<cr>
```

The first and third files must have been created prior to this execution. They contain input data used by the program. The second file may be created during execution. The FILENAMES must be legal TOPS-20 file names; they are limited to eight characters by an internal buffer in CS1.

A. FILES

- 1) File1 contains data for each point to be calculated. The file format is shown below.
- 2) File2 is an empty file for output of plotting data if the plots are to be saved. This file name must be entered even if no plotting is to be done. TOPS-20 will create the file if plotting data is to be stored; other operating systems may require the file to be created before the run begins.
- 3) File3 contains a table of channel doping profiles.

B. Examples of FILE FORMATS.

Each point to be calculated requires 5 lines of input. Data on a given line is free-format. Comments may appear after all required data fields. After each point is calculated, the program will look for additional data until a source doping of zero is found (first line of input), after which the program will terminate.

EXAMPLE OF File1: Data is in units given.

Line 1:

Source doping/cm**3

3.0e19

Line 2:

Vertical junction depth(um),Lateral junction depth(um),Poly-Si length(um)

note: Channel length = Poly-Si length-2*Lateral junction depths

0.55 0.84 5.00

Line 3:

Drain(volts),Gate(volts),Substrate(volts)

note: Source voltage = 0.0.

0.15 +1.158 0.0

Line 4:
Oxide thickness(um),Oxide dielectric constant,Interface charge(cm**2)
0.057 4.0 0.0

Line 5:
Channel mobility(cm**2/V-sec),Channel width(um)
400.0 20.0

Line 6:
Line 6 may contain 0.0 for stopping program, or may be
first line of data for next point to be calculated. Last line in
data file must be zero.

EXAMPLE of File3: Data for doping density.

Line 1:
Contains integer, Ndop, denoting the length of the profile table.

2
Lines 2 through Ndop+1:
Each contains an x (um) and the doping density at x (1/cm**3)
0.0 3.e15
100.0 3.e15

C. OUTPUT DISPLAY

All outputs (except the drain current) are in intrinsic Debye lengths (33um) and thermal volts (25mV), or units derived from these such as, Thermal volts/Debye length.

1. After program execution, the following prompts appear on the display:

ENTER 0,1,2,3 FOR CURRENT AND NEXT POINT, 2D PRINTING,
2D PLOTTING, CURRENT AND STOPPING.

- 0 -- print current. Continue to next point in data file, if any.
- 1 -- print additional information about point just calculated.
- 2 -- plot additional information about point just calculated.
- 3 -- print current and terminate execution. Do not continue to next data point in data file, if any.

If response 1 or 2 is given, further prompts will be furnished.

2. OPTIONS for printing (response 1)

The prompt is
ENTER SUMMARY,NX,NY

- SUMMARY -- for a summary of the number of mesh points and triangles created, how much memory allocated, and how much time used, enter 1. If not desired, enter 0.
- NX & NY -- how many points along X and Y are to be printed in the print matrix. If NX and NY are both negative, a scaled integer printer plot of the potential will result. If NX and NY are both positive, a rectangular grid is

placed on the region; at each point X, Y, U (the potential), UX, and UY (the derivatives of U in the X and Y directions) will be printed. At grid points outside the region, large numbers will be printed.

3. OPTIONS for plotting (response 2)

The prompt is

1:TRIANGLES, 2:CONTOURS, 3:SURFACE, 4:PROFILES

Enter 1, 2, 3, or 4, to plot on screen.

Enter 101, 102, 103, or 104, to save plot data on File2.

Enter 0 to terminate plotting.

Each plot mode will furnish one or more further prompts. In every screen-plotting case, the final prompt before drawing the plot is

Enter g or G to when ready to plot

This gives the user time to clear the screen or to do any work necessary to put the terminal in plotting mode.

After each plot is drawn on the screen, the program will wait for a carriage return, and then re-issue the above prompt. This gives the user time to clear the screen or to do any work necessary to change the terminal out of plotting mode.

1: TRIANGLE PLOTS

The prompt is

ENTER LEVEL

Enter level number (1, 2, ...) to plot the mesh of that level.

Enter 0 to terminate triangle plotting.

After the triangle plot has been drawn, the program waits for a carriage return, and then reissues the Triangle Plot prompt.

2: CONTOUR PLOTS

The first prompt is

1:FUNCTION, 2:ABS(GRADIENT)

Enter 1 to plot the function (potential), or 2 to plot the absolute value of its gradient (absolute value of electric field; units are thermal volts/Debye length).

Enter 0 to terminate contour plotting.

The next prompt is

NUMBER OF CONTOURS

Enter the number of contour lines to be drawn. They will be drawn equally-spaced between (and including) the minimum and maximum values found.

After the contour plot has been drawn, the program waits for a carriage return, and then reissues the first Contour Plot prompt.

3: SURFACE PLOTS

The first prompt is
1:FUNCTION, 2:ABS(GRAIENT)

Enter 1 to plot the function (potential), or 2 to plot the absolute value of its gradient (absolute value of electric field; units are thermal volts/Debye length).

Enter 0 to terminate surface plotting.

The next prompt is
ENTER LEVEL
Enter level number (1, 2, ...) to make a plot of the surface using the mesh of the given level.
Enter 0 to return to the First Surface Plot prompt

The next prompt is
ENTER VIEWING DIRECTION--NX,NY,NZ
Enter three integers. The surface plot is a (parallel) projection of the surface as seen from indicated direction. Thus (0,0,1) will give a top view (like a Triangle Plot), and (0,-1,0) will give a side view.

After the surface plot has been drawn, the program waits for a carriage return, and then reissues the first Surface Plot prompt.

4: PROFILE PLOTS

The first prompt is
ENTER NUMBER OF PROFILES
Enter an integer, the number of profiles to be drawn.
Enter 0 to terminate profile plotting.

The next prompt is
ENTER INDICES OF PROFILE PLANE(S), NX AND NY
Enter two integers. A profile plot is a slice through the solution, perpendicular to the given direction. Thus (0,1) will give a slice parallel to the X axis.

After the profile plot has been drawn, the program waits for a carriage return, and then reissues the first Profile Plot prompt.

2. BATCH EXECUTION (for DEC-20 only)

A. Submit File

Create a submit file which contains:

1. RUN CS1.EXE
2. FILENAME1
3. FILENAME2
4. FILENAME3
5. (Any other input used for the the equivalent interactive execution).

B. Output will go to file CS1.LOG which can be examined with the editor.

3. SUMMARY OF MODEL

A two-dimensional charge sheet model of a surface-channel MOS transistor has been developed. When this model is implemented using adaptive finite element methods, an efficient high-accuracy transistor simulation program is possible. The simulations produced using this model have been compared to experimental measurements; the model is in good agreement for transistors with channel lengths as short as 1.12 μ m. In this verification process the model represented accurately the onset of subthreshold current, channel-length-induced threshold voltage offset, and drain-field output conductance changes.

Appendix C
File CS1.EXP

Sample input data (first file)

```
1.E20
0.80 0.59 3.00
0.15 1.158 0.0
0.0570 4.0 0.0e00
416.0 20.0
1.E20
0.80 0.59 3.00
0.15 1.658 0.0
0.0570 4.0 0.0e00
416.0 20.0
0.0
```

Sample input channel profile (third file)

```
2
0.0 1.E15
200.0 1.E15
```

Sample run using data shown above (DEC 20).
In this run all user input is labeled by (user input).

```
@run cs1.exe
INPUT FILE NAME FOR INPUT DATA,
FILE NAME MUST BE <= 8 CHARACTERS.
cs1.dat (user input)
INPUT FILE NAME FOR OUTPUT DATA PLOTTING
cs1.plt (user input)
INPUT FILENAME FOR DOPING PROFILE DATA
cs1.dop (user input)
  BETA = 3.868472E+01
  PSIB = 2.871279E-01
  LB = 1.292317E-05
  COX = 6.210526E-08
  BPS0 = 2.101317E+01
  BPSI = 2.652973E+01
PS(0) = 6.857934E-01
  NO = 9.071783E+10
PS(L) = 8.104595E-01
  NL = 3.404201E+10
  ID = 6.762688E-06
  IO = 1.181714E+02
  I... = 3.564658E+01
  VG = 4.479690E+01
  VSD = 5.802708E+00
  LCH = 5.454411E-02
```

4 FOR CHANNEL PRINTING

1 (user input)
 enter summary,nx,ny
 1 -6 -11 (user input)

3 MULTI-GRID LEVELS

VERTICES	146	387	617
TRIANGLES	322	982	1686

STORAGE ALLOCATION

	ALLOCATED	USED
MAXT	4591	1691
MAXV	1722	617
MAXVSM	2296	1153
MAXJA	9749	4348
MAXU	1099	1099
MAXJU	1099	1062
TOTAL	54686	23223

TIMING DISTRIBUTION

	SECONDS	PERCENT
GRID	0.226	0.118
ASMBLY	103.892	54.249
MG	84.522	44.135
ADAPT	2.870	1.499
TOTAL	191.510	100.000

scaled values from -1.111E+01 to 2.500E+01 scale 2.500E+01

9999 9999	17	-40	-44	-44
9999 9999	12	-42	-44	-44
9999 9999	-2	-43	-44	-44
89 54	-22	-44	-44	-44
100 13	-37	-44	-44	-44
94 -1	-41	-44	-44	-44
88 5	-39	-44	-44	-44
63 38	-29	-44	-44	-44
9999 9999	-12	-44	-44	-44
9999 9999	0	-43	-44	-44
9999 9999	4	-42	-44	-44

ENTER 0 FOR CURRENT AND NEXTPOINT

1 FOR 2D PRINTING

2 FOR 2D PLOTTING

3 FOR CURRENT AND STOPPING

4 FOR CHANNEL PRINTING

1 (user input)

enter summary,nx,ny

0 6 11 (user input)

I	X	Y	U	UX	UY
1	0.00000	0.00000	1.70141E+38	1.70141E+38	1.70141E+38
2	0.01839	0.00000	1.70141E+38	1.70141E+38	1.70141E+38

3	0.03678	0.00000	9.58144E-01	-1.24680E+03	-9.78029E+01
4	0.05517	0.00000	-1.04111E+01	-1.82800E+02	-8.38715E+01
5	0.07355	0.00000	-1.10993E+01	-1.13871E+01	-2.47837E+00
6	0.09194	0.00000	-1.11075E+01	4.58229E-01	2.03329E-01
7	0.00000	0.01253	1.70141E+38	1.70141E+38	1.70141E+38
8	0.01839	0.01253	1.70141E+38	1.70141E+38	1.70141E+38
9	0.03678	0.01253	-7.82947E-02	-1.24951E+03	-1.99585E+02
10	0.05517	0.01253	-1.07115E+01	-8.98376E+01	-5.09973E+00
11	0.07355	0.01253	-1.11026E+01	-7.23250E+00	2.03329E-01
12	0.09194	0.01253	-1.11075E+01	2.46640E-01	0.00000E+00
13	0.00000	0.02505	1.70141E+38	1.70141E+38	1.70141E+38
14	0.01839	0.02505	1.70141E+38	1.70141E+38	1.70141E+38
15	0.03678	0.02505	-3.04848E+00	-1.04036E+03	-3.75744E+02
16	0.05517	0.02505	-1.08778E+01	-5.80910E+01	-6.96095E+00
17	0.07355	0.02505	-1.11101E+01	2.81150E-01	2.59381E-01
18	0.09194	0.02505	-1.11075E+01	-2.32784E-02	0.00000E+00
19	0.00000	0.03758	1.58477E+01	1.79824E+03	4.59544E+03
20	0.01839	0.03758	9.53071E+00	-1.01526E+03	-9.01933E+02
21	0.03678	0.03758	-7.12977E+00	-5.72754E+02	-2.55661E+02
22	0.05517	0.03758	-1.10460E+01	-5.12203E+01	-3.48379E+01
23	0.07355	0.03758	-1.11071E+01	5.61262E-03	-5.07924E-03
24	0.09194	0.03758	-1.11075E+01	-1.92022E-02	0.00000E+00
25	0.00000	0.05011	2.20992E+01	-1.44968E+03	1.27753E+02
26	0.01839	0.05011	1.27613E+00	-8.08550E+02	-3.37286E+02
27	0.03678	0.05011	-9.83393E+00	-2.56518E+02	-1.56215E+02
28	0.05517	0.05011	-1.10851E+01	-1.14023E+01	-8.79710E+00
29	0.07355	0.05011	-1.11074E+01	5.61262E-03	-2.44136E-01
30	0.09194	0.05011	-1.11075E+01	-7.34552E-03	0.00000E+00
31	0.00000	0.06264	2.35587E+01	-1.60102E+03	1.26531E+02
32	0.01839	0.06264	-3.05892E-01	-8.09359E+02	9.27894E+01
33	0.03678	0.06264	-1.02042E+01	-1.25966E+02	2.96531E+01
34	0.05517	0.06264	-1.11043E+01	-2.24213E+00	8.89146E+00
35	0.07355	0.06264	-1.11076E+01	1.89679E-01	-1.47744E-02
36	0.09194	0.06264	-1.11075E+01	-7.34552E-03	0.00000E+00
37	0.00000	0.07516	2.49961E+01	-1.49096E+03	1.00300E+02
38	0.01839	0.07516	3.18066E+00	-8.78082E+02	4.96746E+02
39	0.03678	0.07516	-9.27189E+00	-3.46915E+02	2.35055E+02
40	0.05517	0.07516	-1.10720E+01	-1.86051E+01	1.51825E+01
41	0.07355	0.07516	-1.11074E+01	1.20671E-03	2.49914E-01
42	0.09194	0.07516	-1.11075E+01	-7.34552E-03	0.00000E+00
43	0.00000	0.08769	2.22886E+01	1.46264E+03	-3.13579E+03
44	0.01839	0.08769	1.35906E+01	-1.14082E+03	1.08186E+03
45	0.03678	0.08769	-5.55180E+00	-7.11942E+02	3.34245E+02
46	0.05517	0.08769	-1.09763E+01	-4.73173E+01	2.89867E+01
47	0.07355	0.08769	-1.11088E+01	1.20671E-03	-1.45270E-01
48	0.09194	0.08769	-1.11075E+01	-1.94337E-02	0.00000E+00
49	0.00000	0.10022	1.70141E+38	1.70141E+38	1.70141E+38
50	0.01839	0.10022	1.70141E+38	1.70141E+38	1.70141E+38
51	0.03678	0.10022	-5.58964E-01	-1.21393E+03	4.47622E+02
52	0.05517	0.10022	-1.06938E+01	-8.02369E+01	3.40412E+01
53	0.07355	0.10022	-1.11140E+01	-3.81814E+00	-9.89015E-01
54	0.09194	0.10022	-1.11075E+01	9.71475E-02	0.00000E+00

55	0.00000	0.11274	1.70141E+38	1.70141E+38	1.70141E+38
56	0.01839	0.11274	1.70141E+38	1.70141E+38	1.70141E+38
57	0.03678	0.11274	3.00789E+00	-1.44263E+03	2.27028E+02
58	0.05517	0.11274	-1.03946E+01	-1.50872E+02	1.31435E+01
59	0.07355	0.11274	-1.11073E+01	-2.80341E+00	2.98414E+00
60	0.09194	0.11274	-1.11075E+01	1.12634E+00	0.00000E+00
61	0.00000	0.12527	1.70141E+38	1.70141E+38	1.70141E+38
62	0.01839	0.12527	1.70141E+38	1.70141E+38	1.70141E+38
63	0.03678	0.12527	4.26292E+00	-1.42063E+03	1.20125E+02
64	0.05517	0.12527	-9.91306E+00	-2.91113E+02	1.18065E+02
65	0.07355	0.12527	-1.10732E+01	-4.72232E-01	7.43968E-01
66	0.09194	0.12527	-1.11075E+01	-1.97903E+00	2.98414E+00

ENTER 0 FOR CURRENT AND NEXTPOINT

1 FOR 2D PRINTING

2 FOR 2D PLOTTING

3 FOR CURRENT AND STOPPING

4 FOR CHANNEL PRINTING

2 (user input)

1:triangles, 2:contours, 3:surface, 4:profiles

1 (user input)

enter level

1 (user input)

enter g or G when ready to plot

g (user input)

(See figure C-1 for graphic output)

Lenter g or g when ready to plot

g (user input)

enter level

2 (user input)

enter g or G when ready to plot

g (user input)

(See figure C-2 for graphic output)

enter g or G when ready to plot

g (user input)

enter level

3 (user input)

enter g or G when ready to plot

g (user input)

(See figure C-3 for graphic output)

enter g or G when ready to plot

g (user input)

enter level

0 (user input)

1:triangles, 2:contours, 3:surface, 4:profiles

3 (user input)

1:function, 2:abs(gradient)

1 (user input)

enter level

1 (user input)

enter viewing direction -- nx,ny,nz

3 -1 1 (user input)

enter g or G when ready to plot

g (user input)

```

(See figure C-4 for graphic output)
enter g or G when ready to plot
g (user input)
1:function, 2:abs(gradient)
1 (user input)
enter level
2 (user input)
enter viewing direction -- nx,ny,nz
3 -1 1 (user input)
enter g or G when ready to plot
g (user input)
(See figure C-5 for graphic output)
enter g or G when ready to plot
g (user input)
1:function, 2:abs(gradient)
1 (user input)
enter level
3 (user input)
enter viewing direction -- nx,ny,nz
3 -1 1 (user input)
enter g or G when ready to plot
g (user input)
(See figure C-6 for graphic output)
enter g or G when ready to plot
g (user input)
1:function, 2:abs(gradient)
0 (user input)
1:triangles, 2:contours, 3:surface, 4:profiles
2 (user input)
1:function, 2:abs(gradient)
1 (user input)
number of contours
-8 (user input)
umin and umax
-10 25 (user input)
ulev
  -1.000E+01   5.000E+00   0.000E+00   5.000E+00   1.000E+01
   1.500E+01   2.000E+01   2.500E+01
enter g or G when ready to plot
g (user input)
(See figure C-7 for graphic output)
enter g or G when ready to plot
g (user input)
1:function, 2:abs(gradient)
0 (user input)
1:triangles, 2:contours, 3:surface, 4:profiles
0 (user input)
ENTER 0 FOR CURRENT AND NEXTPOINT
      1 FOR 2D PRINTING
      2 FOR 2D PLOTTING
      3 FOR CURRENT AND STOPPING
      4 FOR CHANNEL PRINTING
0 (user input)

```

normalized current 3.90387E+07 current 1.61832E-05 15-2.23085E-01

BETA = 3.868472E+01
PSIB = 2.871279E-01
LB = 1.292317E-05
COX = 6.210526E-08
BPSO = 2.101317E+01
BPSI = 2.810985E+01
PS(0) = 7.266396E-01
NO = 2.659051E+11
PS(L) = 8.694479E-01
NL = 2.012935E+11
ID = 2.564667E-05
IO = 1.181714E+02
I... = 1.351853E+02
VG = 6.413927E+01
VSD = 5.802708E+00
LCH = 5.454411E-02

level 1

1	dpsi	-1.421E+01	a	-4.181E+06	umax	3.953E+01
2	dpsi	1.567E+01	a	-3.541E+08	umax	1.835E+01
3	dpsi	-1.018E+00	a	-2.516E+08	umax	8.423E+00
4	dpsi	-1.028E+00	a	-1.643E+08	umax	5.007E+00
5	dpsi	-1.041E+00	a	-1.297E+08	umax	4.235E+00
6	dpsi	-1.057E+00	a	-1.233E+08	umax	1.060E+00
7	dpsi	-1.057E+00	a	-1.246E+08	umax	1.060E+00
8	dpsi	-1.057E+00	a	-1.230E+08	umax	1.060E+00
9	dpsi	-1.014E+00	a	-1.179E+08	umax	1.016E+00
10	dpsi	-9.497E-01	a	-1.117E+08	umax	9.503E-01
11	dpsi	-8.875E-01	a	-1.060E+08	umax	8.911E-01
12	dpsi	-7.569E-01	a	-1.014E+08	umax	7.653E-01
13	dpsi	-5.473E-01	a	-9.766E+07	umax	5.573E-01
14	dpsi	-3.251E-01	a	-9.461E+07	umax	3.286E-01
15	dpsi	-8.178E-04	a	-9.460E+07	umax	2.110E-01

level 2

1	dpsi	7.274E-02	a	-9.511E+07	umax	2.110E-01
2	dpsi	8.938E-01	a	-9.898E+07	umax	2.595E+00
3	dpsi	-5.622E-01	a	-9.256E+07	umax	7.611E-01
4	dpsi	-4.720E-01	a	-9.026E+07	umax	6.152E-01
5	dpsi	-3.972E-01	a	-8.976E+07	umax	4.997E-01
6	dpsi	-3.338E-01	a	-8.998E+07	umax	4.071E-01
7	dpsi	-2.794E-01	a	-9.034E+07	umax	3.320E-01
8	dpsi	-2.329E-01	a	-9.056E+07	umax	2.708E-01
9	dpsi	-1.933E-01	a	-9.058E+07	umax	2.208E-01
10	dpsi	-1.600E-01	a	-9.048E+07	umax	1.834E-01
11	dpsi	-1.321E-01	a	-9.034E+07	umax	1.539E-01
12	dpsi	-1.090E-01	a	-9.022E+07	umax	1.294E-01
13	dpsi	-9.146E-02	a	-9.014E+07	umax	1.090E-01
14	dpsi	-7.847E-02	a	-9.010E+07	umax	9.195E-02
15	dpsi	-6.725E-02	a	-9.007E+07	umax	7.772E-02

level 3

1	dpsi	-2.044E-02	a	-9.016E+07	umax	7.772E-02
2	dpsi	-6.264E-01	a	-8.872E+07	umax	2.303E+00

3	dpsi	-6.057E-01	a	-9.076E+07	umax	6.299E-01
4	dpsi	-5.519E-01	a	-9.087E+07	umax	5.671E-01
5	dpsi	-4.956E-01	a	-9.052E+07	umax	5.175E-01
6	dpsi	-4.541E-01	a	-9.032E+07	umax	4.759E-01
7	dpsi	-4.178E-01	a	-9.029E+07	umax	4.396E-01
8	dpsi	-3.854E-01	a	-9.032E+07	umax	4.071E-01
9	dpsi	-3.561E-01	a	-9.032E+07	umax	3.775E-01
10	dpsi	-3.294E-01	a	-9.029E+07	umax	3.502E-01
11	dpsi	-3.049E-01	a	-9.023E+07	umax	3.249E-01
12	dpsi	-2.824E-01	a	-9.017E+07	umax	3.015E-01
13	dpsi	-2.616E-01	a	-9.012E+07	umax	2.798E-01
14	dpsi	-2.424E-01	a	-9.007E+07	umax	2.597E-01
15	dpsi	-2.246E-01	a	-9.003E+07	umax	2.411E-01

ENTER 0 FOR CURRENT AND NEXTPOINT

1 FOR 2D PRINTING

2 FOR 2D PLOTTING

3 FOR CURRENT AND STOPPING

4 FOR CHANNEL PRINTING

1 (user input)

enter summary,nx,ny

1 11 11 (user input)

3 MULTI-GRID LEVELS

VERTICES	146	403	613
TRIANGLES	322	1028	1676

STORAGE ALLOCATION

	ALLOCATED	USED
MAXT	4591	1681
MAXV	1722	613
MAXVSM	2296	1165
MAXJA	9749	4396
MAXU	1099	1099
MAXJU	1099	1062
TOTAL	54686	23301

TIMING DISTRIBUTION

	SECONDS	PERCENT
GRID	0.232	0.119
ASMBLY	105.177	53.804
MG	86.983	44.497
ADAPT	3.090	1.581
TOTAL	195.482	100.000

I	X	Y	U	UX	UY
1	0.00000	0.00000	1.70141E+38	1.70141E+38	1.70141E+38
2	0.00919	0.00000	1.70141E+38	1.70141E+38	1.70141E+38
3	0.01839	0.00000	1.70141E+38	1.70141E+38	1.70141E+38
4	0.02758	0.00000	1.57054E+01	-1.91704E+03	-1.00523E+02
5	0.03678	0.00000	9.65422E-01	-1.24682E+03	-9.76190E+01
6	0.04597	0.00000	-7.26674E+00	-6.01051E+02	-1.08911E+02

7	0.05517	0.00000	-1.04098E+01	-1.83119E+02	-8.39450E+01
8	0.06436	0.00000	-1.09944E+01	-1.14218E+01	-2.47309E+00
9	0.07355	0.00000	-1.10994E+01	-1.14218E+01	-2.47309E+00
10	0.08275	0.00000	-1.11117E+01	4.65918E-01	2.09808E-01
11	0.09194	0.00000	-1.11075E+01	4.65918E-01	2.09808E-01
12	0.00000	0.01253	1.70141E+38	1.70141E+38	1.70141E+38
13	0.00919	0.01253	1.70141E+38	1.70141E+38	1.70141E+38
14	0.01839	0.01253	1.70141E+38	1.70141E+38	1.70141E+38
15	0.02758	0.01253	1.47769E+01	-2.08413E+03	-8.83702E+01
16	0.03678	0.01253	-6.45350E-02	-1.25021E+03	-1.98808E+02
17	0.04597	0.01253	-8.00539E+00	-4.72531E+02	-3.76761E+01
18	0.05517	0.01253	-1.07103E+01	-9.00897E+01	-5.09873E+00
19	0.06436	0.01253	-1.10358E+01	-7.26375E+00	2.09808E-01
20	0.07355	0.01253	-1.11026E+01	-7.26375E+00	2.09808E-01
21	0.08275	0.01253	-1.11097E+01	2.47587E-01	0.00000E+00
22	0.09194	0.01253	-1.11075E+01	2.47587E-01	0.00000E+00
23	0.00000	0.02505	1.70141E+38	1.70141E+38	1.70141E+38
24	0.00919	0.02505	1.70141E+38	1.70141E+38	1.70141E+38
25	0.01839	0.02505	1.70141E+38	1.70141E+38	1.70141E+38
26	0.02758	0.02505	9.52872E+00	-1.81628E+03	-8.72109E+02
27	0.03678	0.02505	-3.03173E+00	-1.03973E+03	-3.72893E+02
28	0.04597	0.02505	-9.16492E+00	-3.18113E+02	-8.87428E+01
29	0.05517	0.02505	-1.08767E+01	-5.83974E+01	-6.99410E+00
30	0.06436	0.02505	-1.10863E+01	-7.26375E+00	-6.99410E+00
31	0.07355	0.02505	-1.11101E+01	2.96845E-01	2.71334E-01
32	0.08275	0.02505	-1.11077E+01	2.47587E-01	2.71334E-01
33	0.09194	0.02505	-1.11075E+01	-3.47702E-02	0.00000E+00
34	0.00000	0.03758	1.72286E+01	1.17692E+03	4.87063E+03
35	0.00919	0.03758	1.81529E+01	-8.54785E+02	-1.09740E+03
36	0.01839	0.03758	9.68705E+00	-1.02134E+03	-8.89039E+02
37	0.02758	0.03758	-8.99877E-02	-1.11267E+03	-8.57369E+02
38	0.03678	0.03758	-7.08274E+00	-5.77684E+02	-2.55017E+02
39	0.04597	0.03758	-1.04765E+01	-6.02732E+01	-3.92674E+01
40	0.05517	0.03758	-1.10444E+01	-5.21483E+01	-3.52405E+01
41	0.06436	0.03758	-1.11096E+01	2.96845E-01	2.03711E-01
42	0.07355	0.03758	-1.11071E+01	9.63477E-02	-4.61240E-02
43	0.08275	0.03758	-1.11072E+01	-3.47702E-02	-4.61240E-02
44	0.09194	0.03758	-1.11075E+01	2.24505E-03	0.00000E+00
45	0.00000	0.05011	2.31712E+01	-1.51404E+03	1.07122E+02
46	0.00919	0.05011	1.09044E+01	-1.02262E+03	-2.42571E+02
47	0.01839	0.05011	1.65833E+00	-8.28871E+02	-3.25365E+02
48	0.02758	0.05011	-5.55641E+00	-5.65257E+02	-3.50660E+02
49	0.03678	0.05011	-9.77549E+00	-2.66561E+02	-1.58139E+02
50	0.04597	0.05011	-1.09121E+01	-5.65621E+01	-1.53389E+01
51	0.05517	0.05011	-1.10835E+01	-1.11795E+01	-5.04539E+00
52	0.06436	0.05011	-1.11083E+01	9.63477E-02	1.93562E-01
53	0.07355	0.05011	-1.11074E+01	9.63477E-02	1.93562E-01
54	0.08275	0.05011	-1.11075E+01	2.24505E-03	-7.86801E-05
55	0.09194	0.05011	-1.11075E+01	2.30819E-03	0.00000E+00
56	0.00000	0.06264	2.46360E+01	-1.64415E+03	1.24823E+02
57	0.00919	0.06264	1.05622E+01	-1.31833E+03	8.54931E+01
58	0.01839	0.06264	1.47207E-01	-8.31568E+02	9.46786E+01
59	0.02758	0.06264	-6.78125E+00	-6.32757E+02	1.46283E+02

60	0.03678	0.06264	-1.01494E+01	-1.40768E+02	2.95493E+01
61	0.04597	0.06264	-1.09480E+01	-4.17099E+01	6.84505E+01
62	0.05517	0.06264	-1.11023E+01	-1.51335E+00	2.04004E+00
63	0.06436	0.06264	-1.11069E+01	-5.90518E-02	-7.86801E-05
64	0.07355	0.06264	-1.11074E+01	-5.90518E-02	-7.86801E-05
65	0.08275	0.06264	-1.11075E+01	2.30819E-03	0.00000E+00
66	0.09194	0.06264	-1.11075E+01	2.30819E-03	0.00000E+00
67	0.00000	0.07516	2.59830E+01	-1.53400E+03	8.44740E+01
68	0.00919	0.07516	1.32984E+01	-1.08408E+03	4.79736E+02
69	0.01839	0.07516	3.56422E+00	-8.95785E+02	4.86827E+02
70	0.02758	0.07516	-4.30413E+00	-6.39271E+02	4.65338E+02
71	0.03678	0.07516	-9.20783E+00	-3.58072E+02	2.36151E+02
72	0.04597	0.07516	-1.07994E+01	-8.72578E+01	2.58347E+01
73	0.05517	0.07516	-1.10703E+01	-1.83162E+01	1.09657E+01
74	0.06436	0.07516	-1.11084E+01	1.06331E-01	-2.05005E-01
75	0.07355	0.07516	-1.11074E+01	1.06331E-01	-2.05005E-01
76	0.08275	0.07516	-1.11075E+01	1.44525E-03	1.07529E-03
77	0.09194	0.07516	-1.11075E+01	2.30819E-03	0.00000E+00
78	0.00000	0.08769	2.36266E+01	6.81750E+02	-3.01507E+03
79	0.00919	0.08769	2.32034E+01	-9.48153E+02	1.32428E+03
80	0.01839	0.08769	1.37377E+01	-1.14021E+03	1.04329E+03
81	0.02758	0.08769	2.71884E+00	-1.26672E+03	9.99422E+02
82	0.03678	0.08769	-5.52942E+00	-7.16435E+02	3.34261E+02
83	0.04597	0.08769	-9.98166E+00	-1.50930E+02	7.62547E+01
84	0.05517	0.08769	-1.09754E+01	-4.75933E+01	2.90905E+01
85	0.06436	0.08769	-1.10790E+01	-3.83210E+00	4.80330E+00
86	0.07355	0.08769	-1.11088E+01	1.06331E-01	-1.04312E-01
87	0.08275	0.08769	-1.11080E+01	8.51575E-02	-1.04312E-01
88	0.09194	0.08769	-1.11075E+01	1.44525E-03	0.00000E+00
89	0.00000	0.10022	1.70141E+38	1.70141E+38	1.70141E+38
90	0.00919	0.10022	1.70141E+38	1.70141E+38	1.70141E+38
91	0.01839	0.10022	1.70141E+38	1.70141E+38	1.70141E+38
92	0.02758	0.10022	1.37814E+01	-1.98749E+03	9.59081E+02
93	0.03678	0.10022	-4.89539E-01	-1.22193E+03	4.45889E+02
94	0.04597	0.10022	-8.08566E+00	-4.40321E+02	1.25887E+02
95	0.05517	0.10022	-1.06945E+01	-8.01578E+01	3.35411E+01
96	0.06436	0.10022	-1.10436E+01	-1.38424E+01	8.60929E+00
97	0.07355	0.10022	-1.11140E+01	-3.83210E+00	-1.01022E+00
98	0.08275	0.10022	-1.11105E+01	1.13642E+00	-1.01022E+00
99	0.09194	0.10022	-1.11075E+01	8.51575E-02	0.00000E+00
100	0.00000	0.11274	1.70141E+38	1.70141E+38	1.70141E+38
101	0.00919	0.11274	1.70141E+38	1.70141E+38	1.70141E+38
102	0.01839	0.11274	1.70141E+38	1.70141E+38	1.70141E+38
103	0.02758	0.11274	1.97528E+01	-2.29747E+03	1.03905E+02
104	0.03678	0.11274	3.05657E+00	-1.43381E+03	2.32941E+02
105	0.04597	0.11274	-6.61363E+00	-6.41455E+02	4.29263E+01
106	0.05517	0.11274	-1.03770E+01	-1.55745E+02	1.32586E+01
107	0.06436	0.11274	-1.10155E+01	-1.44971E+01	-8.19146E+00
108	0.07355	0.11274	-1.11073E+01	-2.85756E+00	2.99369E+00
109	0.08275	0.11274	-1.11179E+01	1.13642E+00	0.00000E+00
110	0.09194	0.11274	-1.11075E+01	1.13642E+00	0.00000E+00
111	0.00000	0.12527	1.70141E+38	1.70141E+38	1.70141E+38
112	0.00919	0.12527	1.70141E+38	1.70141E+38	1.70141E+38

113	0.01839	0.12527	1.70141E+38	1.70141E+38	1.70141E+38
114	0.02758	0.12527	2.07662E+01	-2.12272E+03	1.01953E+02
115	0.03678	0.12527	4.18054E+00	-1.44197E+03	9.42864E+01
116	0.04597	0.12527	-5.69846E+00	-7.66748E+02	1.21720E+02
117	0.05517	0.12527	-9.95308E+00	-2.76592E+02	1.04345E+02
118	0.06436	0.12527	-1.09852E+01	-4.05405E+01	4.23887E+00
119	0.07355	0.12527	-1.10732E+01	-4.31471E-01	6.62310E-01
120	0.08275	0.12527	-1.10893E+01	-1.97889E+00	2.99369E+00
121	0.09194	0.12527	-1.11075E+01	-1.97889E+00	2.99369E+00

ENTER 0 FOR CURRENT AND NEXTPOINT
 1 FOR 2D PRINTING
 2 FOR 2D PLOTTING
 3 FOR CURRENT AND STOPPING
 4 FOR CHANNEL PRINTING

0 (user input)
 normalized current 9.00330E+07 current 3.73224E-05 15-2.24614E-01
 CPU time 29:18.05 Elapsed time 2:23:34.40

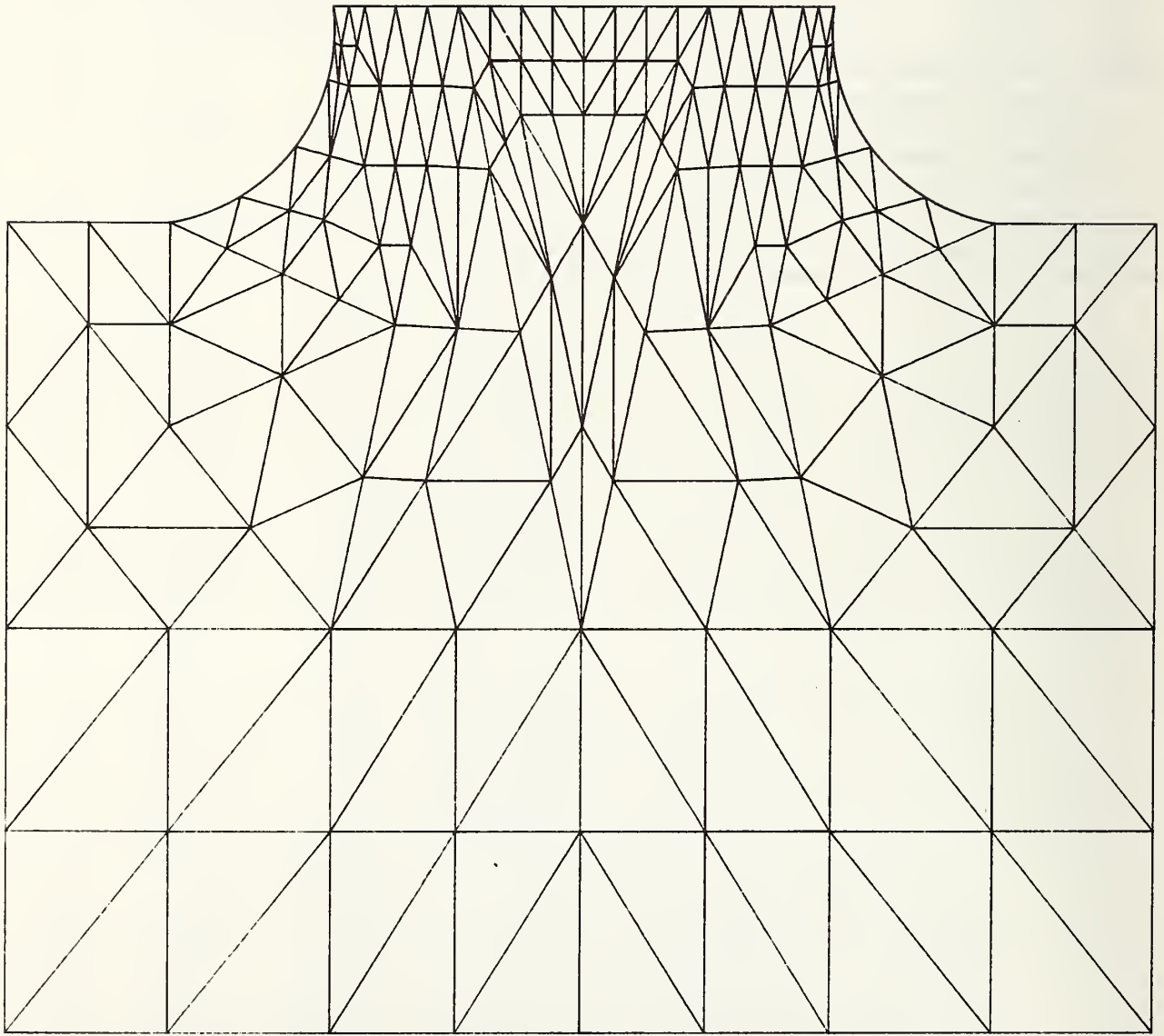


Figure C-1. Example of level 1 mesh.

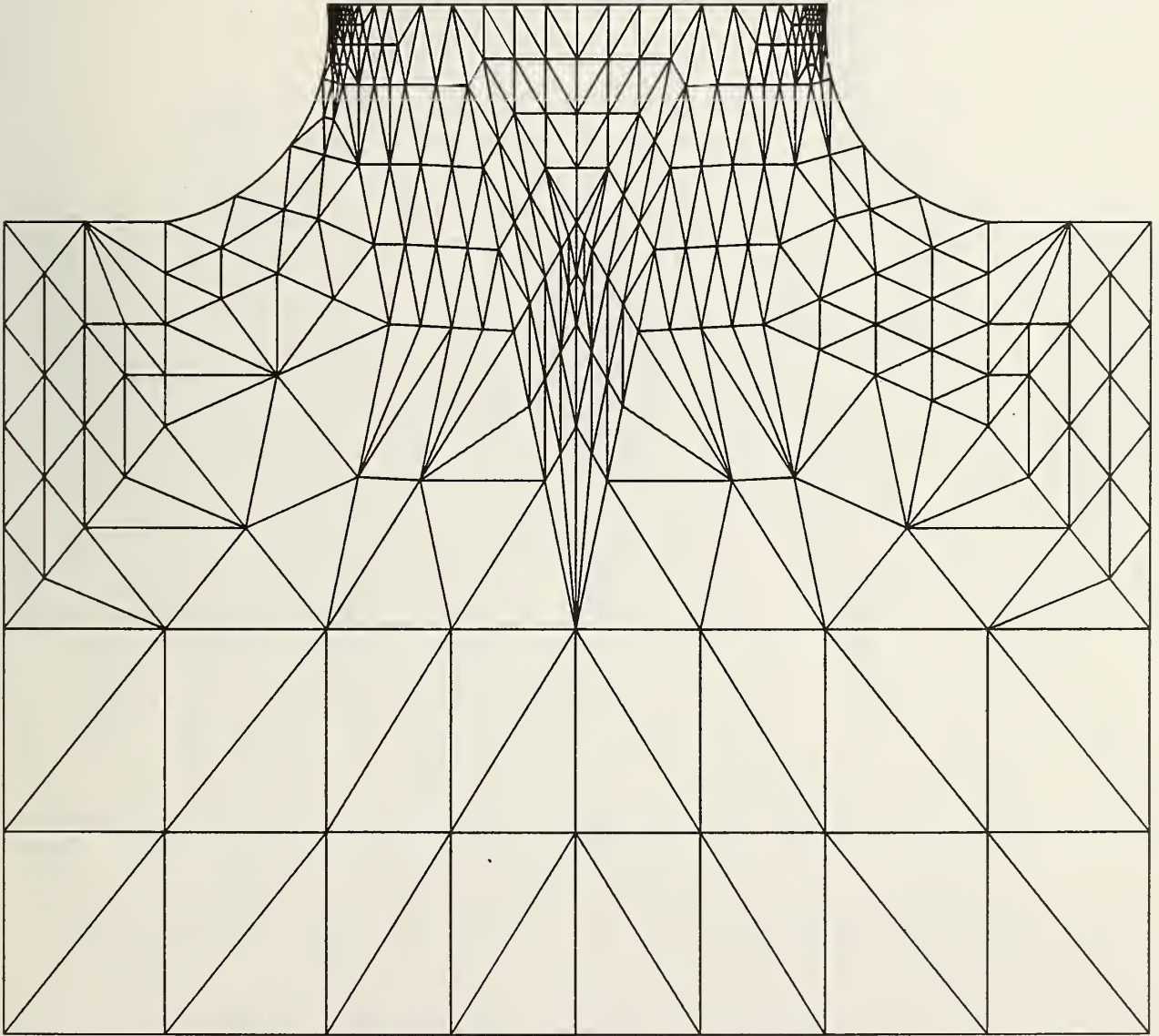


Figure C-2. Example of level 2 mesh.

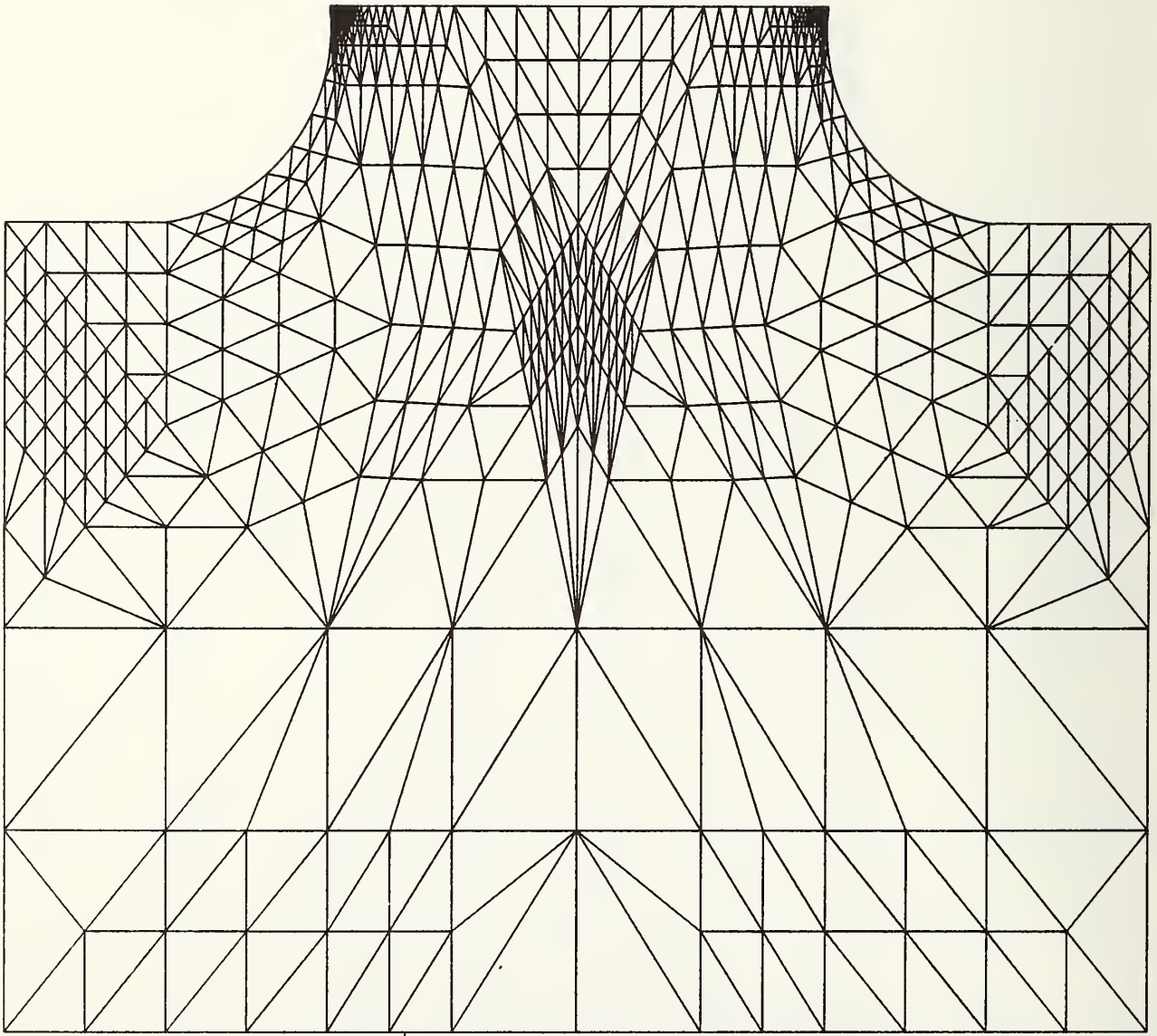


Figure C-3. Example of level 3 mesh.

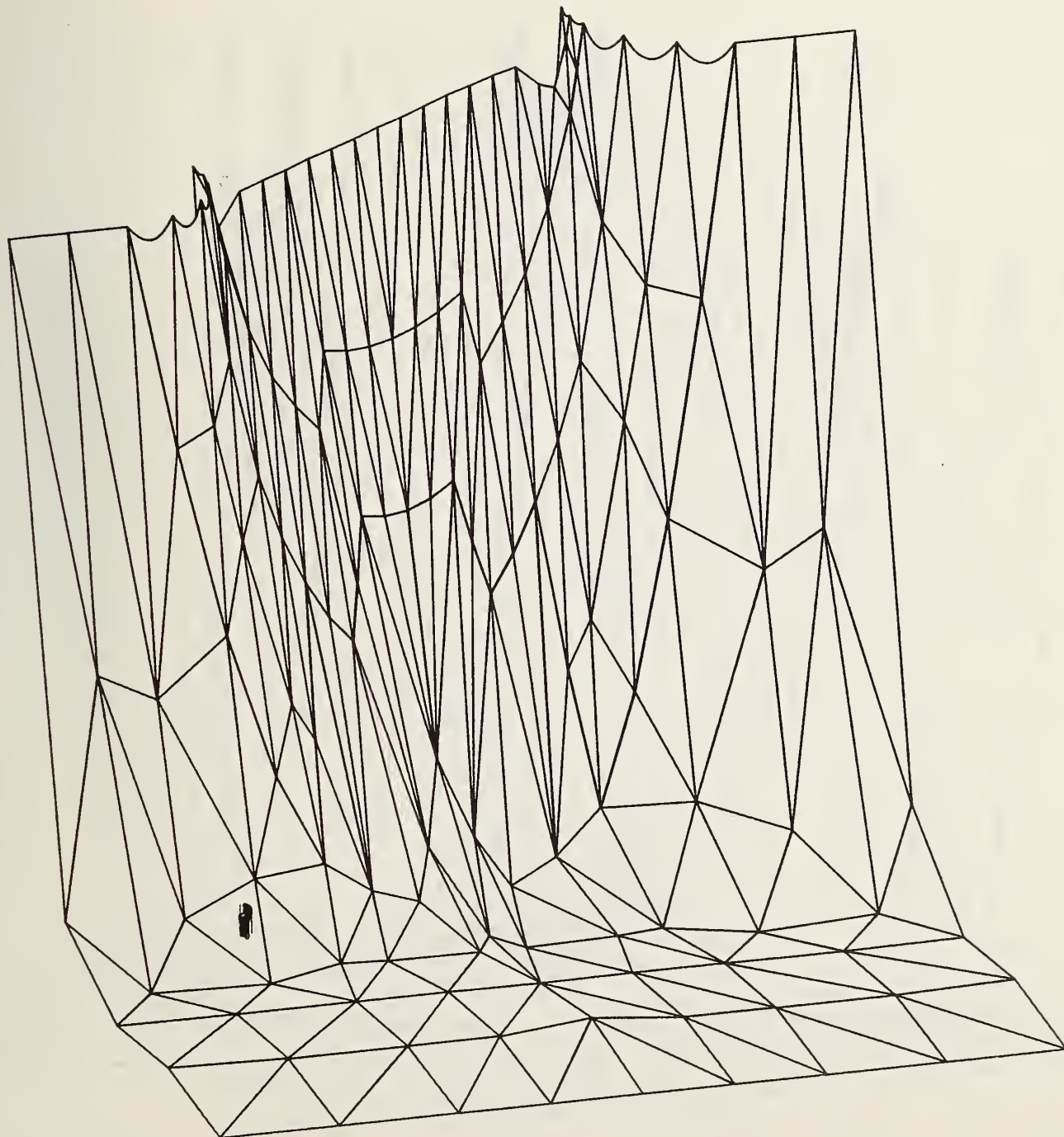


Figure C-4. Example of level 1 projection.

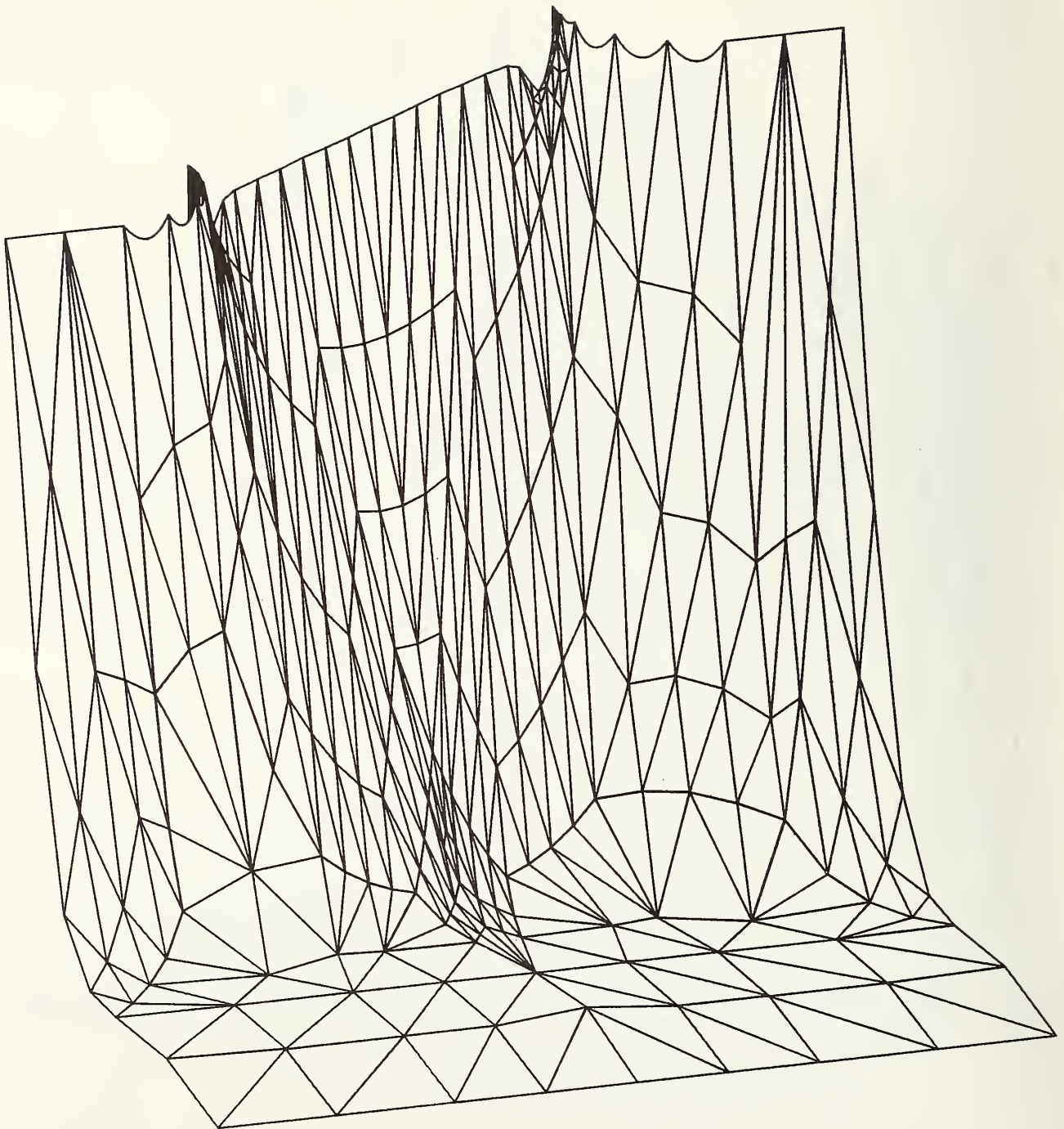


Figure C-5. Example of level 2 projection.

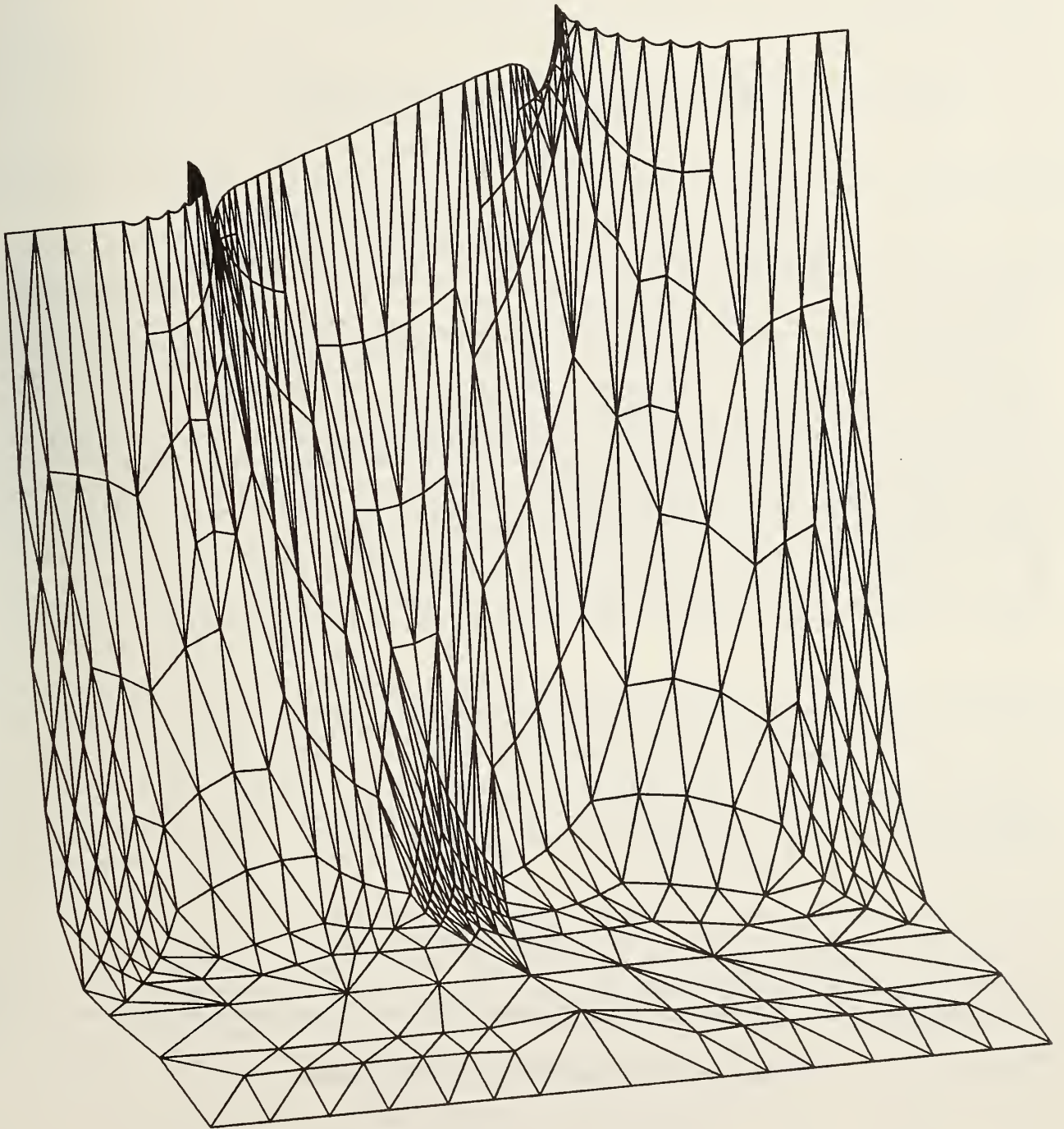


Figure C-6. Example of level 3 projection.

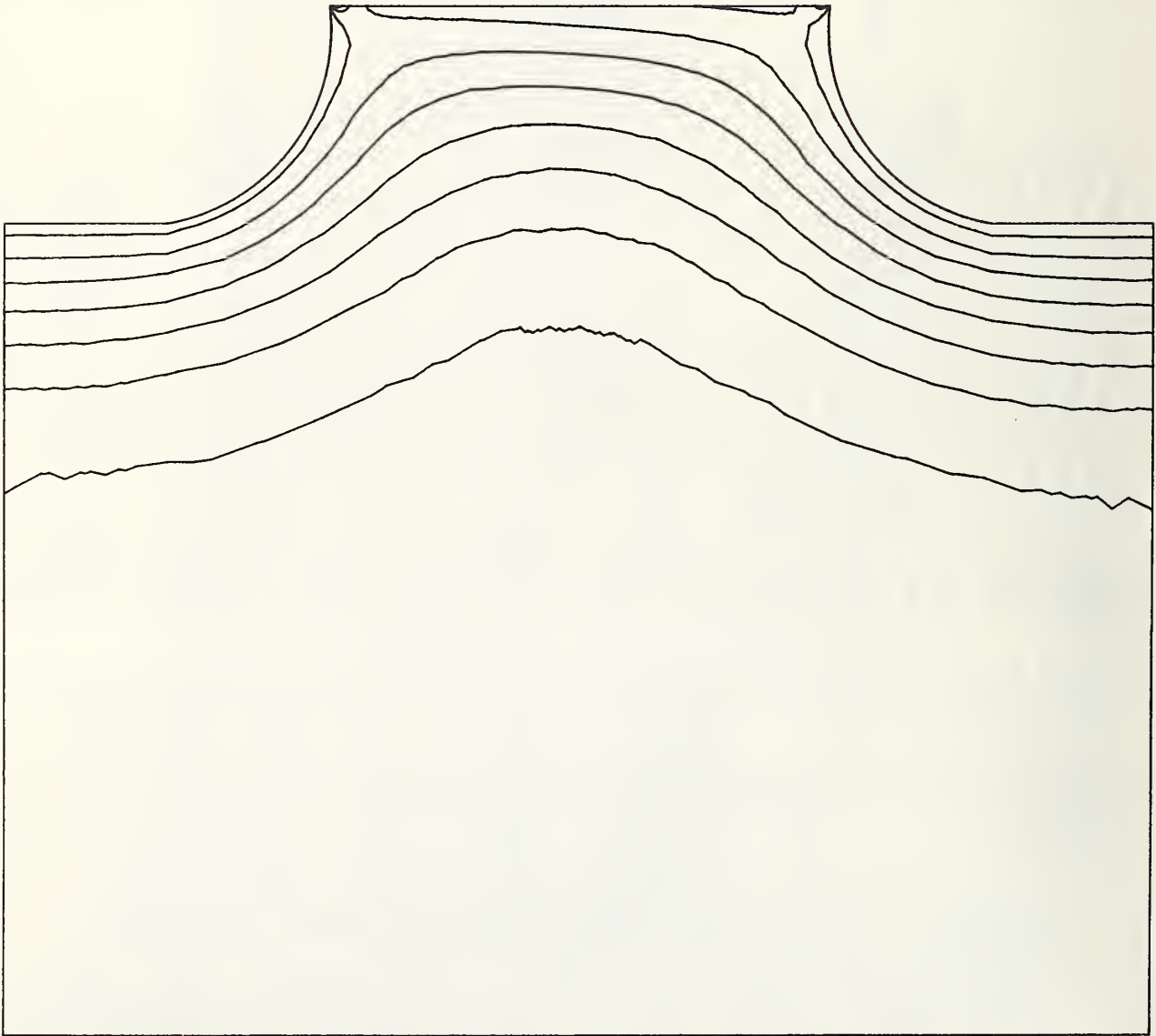


Figure C-7. Example of contour plot.

U.S. DEPT. OF COMM. BIBLIOGRAPHIC DATA SHEET <i>(See instructions)</i>	1. PUBLICATION OR REPORT NO. NBSIR 82-2471	2. Performing Organ. Report No.	3. Publication Date April 1982
4. TITLE AND SUBTITLE CS1: A Two-Dimensional Finite Element Charge-Sheet Model of a Short-Channel MOS Transistor			
5. AUTHOR(S) C. L. Wilson and J. L. Blue			
6. PERFORMING ORGANIZATION <i>(If joint or other than NBS, see instructions)</i> NATIONAL BUREAU OF STANDARDS DEPARTMENT OF COMMERCE WASHINGTON, D.C. 20234		7. Contract/Grant No. 8. Type of Report & Period Covered	
9. SPONSORING ORGANIZATION NAME AND COMPLETE ADDRESS <i>(Street, City, State, ZIP)</i>			
10. SUPPLEMENTARY NOTES <input checked="" type="checkbox"/> Document describes a computer program; SF-185, FIPS Software Summary, is attached.			
11. ABSTRACT <i>(A 200-word or less factual summary of most significant information. If document includes a significant bibliography or literature survey, mention it here)</i> <p>A two-dimensional charge-sheet model for short-channel MOS transistors has been developed. The unique feature of the model is that the effect of channel inversion layer charge is included as a nonlinear integral boundary condition on the two-dimensional electrostatic field in the transistor. The average inversion layer charge density and source-drain current are obtained directly from the model rather than from the electron density or electron quasi-Fermi level. The model retains all of the physical detail of more complex two-dimensional models such as sensitivity to source-drain profile shape, channel profile, and oxide field shape. This allows the model to represent the changes in drain current associated with short-channel effects while still allowing simple comparison with long-channel models. For long-channel transistors, the results of this model are identical to Brews' long-channel charge-sheet model. The accuracy of this model is verified by modeling a sequence of transistors with channel lengths between 4.6 and 1.1 μm. In short-channel transistors, effects previously attributed to high field mobility are explained by simple two-dimensional electrostatics.</p> <p>The simulations produced using this model have been compared to experimental measurements on an array of n-channel MOSFETs; the model is in good agreement for transistors with channel lengths as short as 1.1 μm. In this verification process, the model represented accurately the onset of subthreshold current, channel-length-induced threshold voltage offset, and drain-field-induced output conductance changes.</p> <p>From studies of numerical accuracy, we conclude that the charge-sheet model can easily simulate drain current with an accuracy which exceeds that required for most applications. To obtain 5-percent accuracy for drain current, a 146 element mesh is sufficient. Refinement of the 146 element mesh to a 455 element mesh gives a current which is accurate to 0.16 percent. Average computer time for a high accuracy solution is 2.5 min on a DEC-20.</p> <p>The numerical solutions were obtained using general-purpose software for solving elliptic partial differential equations. Problems with exact solutions have been solved to test the correctness and accuracy of the codes. Also, the physics included in this model and the geometry of the transistor can be easily changed. The finite element method used allows refinement of oblique triangles which is important in achieving computational efficiency. The program is portable and has been run on a DEC-20, a VAX 11/780, a Cyber 175, and a Univac 1108.</p>			
12. KEY WORDS <i>(Six to twelve entries; alphabetical order; capitalize only proper names; and separate key words by semicolons)</i> Elliptic solvers; finite elements; interactive graphics; MOS transistor.			
13. AVAILABILITY <input checked="" type="checkbox"/> Unlimited <input type="checkbox"/> For Official Distribution. Do Not Release to NTIS <input type="checkbox"/> Order From Superintendent of Documents, U.S. Government Printing Office, Washington, D.C. 20402. <input type="checkbox"/> Order From National Technical Information Service (NTIS), Springfield, VA. 22161		14. NO. OF PRINTED PAGES 61 15. Price 9.00	

FEDERAL INFORMATION PROCESSING STANDARD SOFTWARE SUMMARY

01. Summary date			02. Summary prepared by (Name and Phone)			03. Summary action		
Yr.	Mo.	Day	C. L. Wilson (301) 921-3541			New	Replacement	Deletion
8	1	1	05. Software title			<input checked="" type="checkbox"/>	<input type="checkbox"/>	<input type="checkbox"/>
8	1	1				CS1: A Two-Dimensional Finite Element Charge-Sheet Model of a Short-Channel MOS Transistor		
8	1	1	06. Short title					
8	1	1				08. Software type		

08. Software type	09. Processing mode	10. Application area					
Automated Data System <input type="checkbox"/> Computer Program <input checked="" type="checkbox"/> Subroutine/Module <input type="checkbox"/>	Interactive <input checked="" type="checkbox"/> Batch <input checked="" type="checkbox"/> Combination <input type="checkbox"/>	<table style="width: 100%; border-collapse: collapse;"> <tr> <th style="text-align: center; border-bottom: 1px solid black;">General</th> <th style="text-align: center; border-bottom: 1px solid black;">Specific</th> </tr> <tr> <td> Computer Systems Support/Utility <input type="checkbox"/> Scientific/Engineering <input checked="" type="checkbox"/> Bibliographic/Textual <input type="checkbox"/> </td> <td> Management/Business <input type="checkbox"/> Process Control <input type="checkbox"/> Other <input type="checkbox"/> </td> </tr> </table>		General	Specific	Computer Systems Support/Utility <input type="checkbox"/> Scientific/Engineering <input checked="" type="checkbox"/> Bibliographic/Textual <input type="checkbox"/>	Management/Business <input type="checkbox"/> Process Control <input type="checkbox"/> Other <input type="checkbox"/>
General	Specific						
Computer Systems Support/Utility <input type="checkbox"/> Scientific/Engineering <input checked="" type="checkbox"/> Bibliographic/Textual <input type="checkbox"/>	Management/Business <input type="checkbox"/> Process Control <input type="checkbox"/> Other <input type="checkbox"/>						

11. Submitting organization and address	12. Technical contact(s) and phone
National Bureau of Standards Washington, DC 20234	C. L. Wilson 921-3541 J. L. Blue 921-3395

13. Narrative

A two-dimensional charge-sheet model for short-channel MOS transistors has been developed. The unique feature of the model is that the effect of channel inversion layer charge is included as a nonlinear integral boundary condition on the two-dimensional electrostatic field in the transistor. The program is portable and has been run on a DEC-20, a VAX 11/780, a Cyber 275, and a Univac 1108.

14. Keywords

Finite elements, MOS transistor, elliptic solvers, interactive graphics.

15. Computer manuf'r and model	16. Computer operating system	17. Programing language(s)	18. Number of source program statements
DEC-20	TOPS-20	FORTRAN	
19. Computer memory requirements	20. Tape drives	21. Disk/Drum units	22. Terminals
80K	0	0	1

23. Other operational requirements

Requires local vector-oriented graphics

24. Software availability	25. Documentation availability
Available <input checked="" type="checkbox"/> Limited <input type="checkbox"/> In-house only <input type="checkbox"/> C. L. Wilson 921-3541 9-track magnetic tape.	Available <input checked="" type="checkbox"/> Inadequate <input type="checkbox"/> In-house only <input type="checkbox"/> Tital as in section 05.

26. FOR SUBMITTING ORGANIZATION USE

